Depth-dependent Characterization of (Ag,Cu)(In,Ga)Se_2 by X-ray Absorption Spectroscopy

M. Babucci[1], D. M. Meira[2], E. Wallin[3], K. V. Sopiha[1], J. Keller[1], O. Donzel-Gargand[1], C. Platzer Björkman[1], N. M. Martin[1]

[1]Solar Cell Technology, Department of Materials Science and Engineering, Uppsala University, Uppsala 751 21, Sweden
[2]APS Spectroscopy Group, Argonne National Laboratory, Lemont, IL 60439
[3]Solibro Research AB, Uppsala 756 51, Sweden, and Evolar AB, Uppsala, 756 51, Sweden

Cu(In,Ga)Se_2-based (CIGS) solar cells are high-performance thin-film photovoltaic devices renowned for their chemical stability and high light absorption coefficient. Alloying CIGS with silver to form (Ag,Cu)(In,Ga)Se_2 (ACIGS) can further improve the device by improving the crystal quality, increasing the optical bandgap and open-circuit voltage.[1] While the role of Ag on the device performance and crystal structure has already been analyzed,[2] important gaps in our understanding remain, especially with regard to the atomistic (short-range) structure. Specifically, recent studies by X-ray absorption spectroscopy (XAS) have shown that local atomic arrangements in Ag-free CIGS deviate from the long-range crystallographic structure deduced from X-ray diffraction (XRD) measurements.[3] However, it remains to be found how these structural deviations evolve with Ag alloying, particularly in the presence of Ga depth gradient used in the actual absorber films. XAS is an element-specific technique that offers chemical sensitivity to probe local environment of elements. Angular resolved XAS allows for depth-profiling studies and measures sub-nanometer scale structure and compositional variations at varying depths within thin films, minimizing bulk contribution and enables high-sensitivity surface measurements (in grazing incidence mode).[4]

In this work, we employ angle-resolved XAS to probe the local environment of the elements at different depths and at the film surface by varying the incidence angles between 0.05°, 0.5°, and 10°. We analyze several high-performance (~19%) ACIGS devices with overall [Ag]/([Ag]+[Cu]) ratios below 0.2 and a clear compositional Ga gradient. By complementing these results with XRD measurements for the long-range structures, glow discharge optical emission spectroscopy (GDOES) for the elemental profiles, and scanning transmission electron microscopy (STEM) for the morphologies, changes in element-specific bond lengths, cell parameters, and anion displacement depending on compositions of Group [I] (Cu, Ag) and Group [III] (In, Ga) within different depths of samples were mapped. The results suggest that the local atomic arrangement of the investigated (A)CIGS thin film solar cell samples is depth dependent and deviates from the long-range crystallographic structure. Possible reasons for this deviation including anion displacement, tetragonal distortion and/or the presence of other phases or off stoichiometry compounds will be discussed. These findings offer a better understanding of the atomic-scale properties of ACIGS in the actual thin-film solar cells containing in-depth composition variations.

[1] M. Edoff, et al. *IEEE J. Photovol.* 2017, *7*, 1789.
[2] J. H. Boyle et al. *J. Appl. Phys.* 2014, *115*, 223504.
[3] C. S. Schnohr et al. *Acta Materialia* 2018, *153*, 8.
[4] J. Just, D. et al. *APL Mater.* 2017, *5*, 126106.

Depth-dependent Characterization of (Ag,Cu)(In,Ga)Se_2 by X-ray Absorption Spectroscopy

Melike Babucci[1], D. M. Meira[2], E. Wallin[3], K. V. Sopiha[1], J. Keller[1], O. Donzel-Gargand[1], C. Platzer Björkman[1], N. M. Martin[1]

[1] Division of Solar Cell Technology, Department of Materials Science and Engineering, Uppsala University, Sweden
[2] APS Spectroscopy group, ARGONNE National Laboratory, USA
[3] EVOLAR AB, Uppsala, Sweden
melike.babucci@angstrom.uu.se

Why solar power?

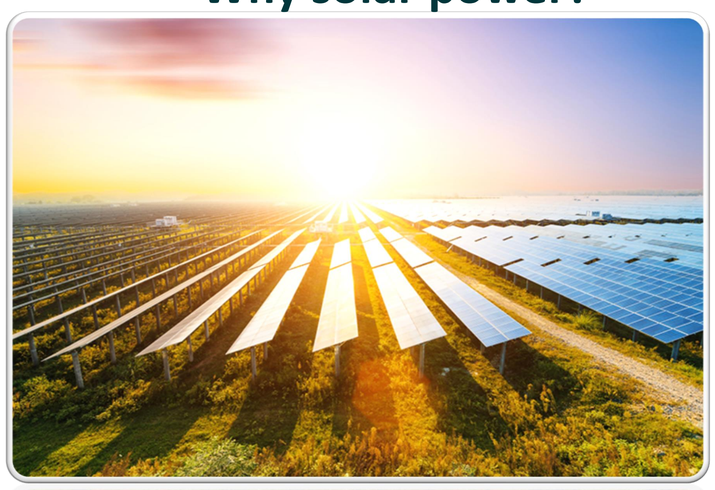

Energy crisis & climate catastrope:
Developments in renewable energy is key importance to transition to net zero by 2050.

- Si solar cells dominate the solar market (95%)
  - However; high material consumption &
  - High energy payback time (years)

Motivation

TFSCs cannot yet compete with fossil fuels due to high cost. For high-efficiency solar cells, understanding their structure-performance relationship **at atomic level through advanced synchrotron techniques** is crucial.

Aim

Investigation of structural deviations between local atomic arrangements in the TFSCs and long-range crystallographic structure and how they evolve with alloying, which can pave the way for high band gap applications such as tandem solar cells by increasing optical bandgap and open-circuit voltage.

Thin film solar cells

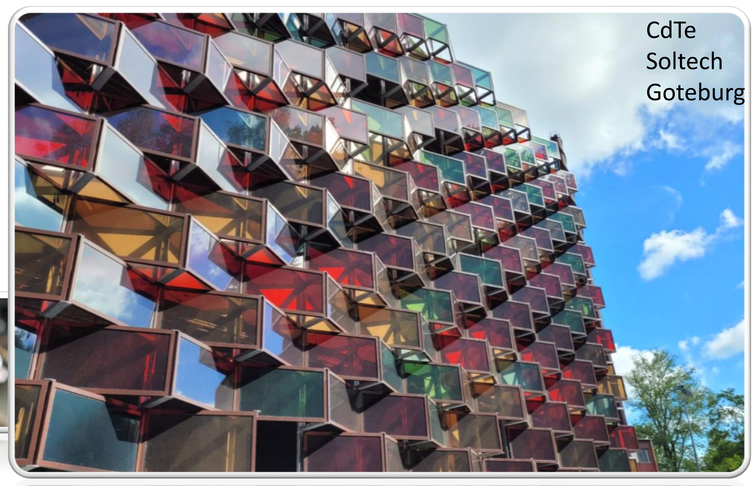

- Low material consumption: cheaper
- Flexible, semi-transparent, light-weight
- Short energy payback time ~5-10 months
- Commercially available
- Good efficiency: a-Si: 14.0%,
  CdTe: 22.1%, Cu(In,Ga)Se_2: 23.4%

Device synthesis & characterization

- $CuInGaSe_2$ (CIGS) and (Ag,Cu)(In,Ga)Se_2 (ACIGS) devices with varying Ag/(Ag+Cu) (AAC) and Ga/(Ga+In) (GGI) ratios were synthesized by Solibro AB
- Deposited Ag replaces Cu atoms in the structure

Sample compositions by XRF

Sample	Cu%	In%	Ga%	Se%	Ag%	I/III	Ga/III	Ag/(Ag+Cu)
CIGS	23.2	15.2	10.3	51.4	0	0.91	0.40	0
ACIGS-0.05	21.4	16.3	8.8	52.3	1.3	0.90	0.35	0.05
ACIGS-0.10	20.3	16.2	8.8	52.5	2.3	0.90	0.35	0.10
ACIGS-0.20	17.8	16.6	8.9	52.7	4.1	0.86	0.35	0.19

Glow discharge optical emission spectroscopy

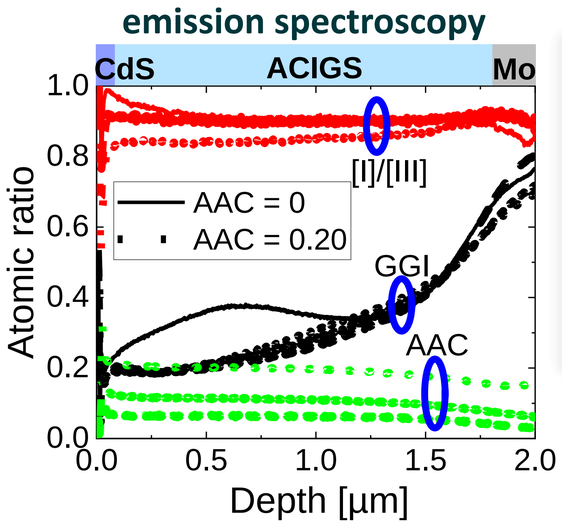

STEM annular dark field images

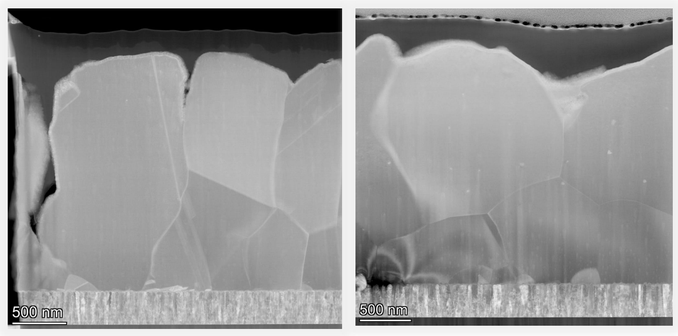

CIGS ACIGS-0.20

- Ga and Ag composition profile within the ACIGS absorbers vary: likely to influence the local atomic structure
- Slightly larger grains in the samples containing Ag

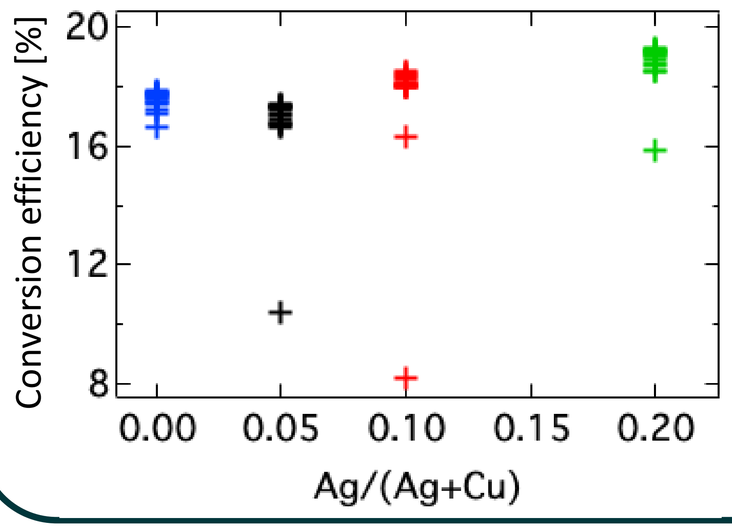

Device performance

Power conversion efficiency of CIGS thin film solar cells increase to ~20% with Ag alloying.

X-ray absorption spectroscopy experiments

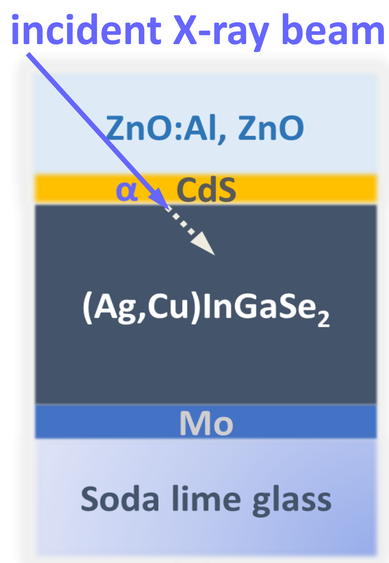

- Accurate probe of chemical, electronic and geometric structures
  - Compositional changes, bond disoNeighboring atom species, distances, and coordination numbers
  - Oxidation state, coordination chemistry, and bond lengths

Angle-resolved XAS allows investigation of compositional and structural changes at different probing depths from the surface of films

- **α = 10°** (~2000 nm)
- **α = 0.5°** (~120-130)
- **α = 0.05°** (~3-5 nm)

More pronounced effect of Ag allying near the film surface

EXAFS

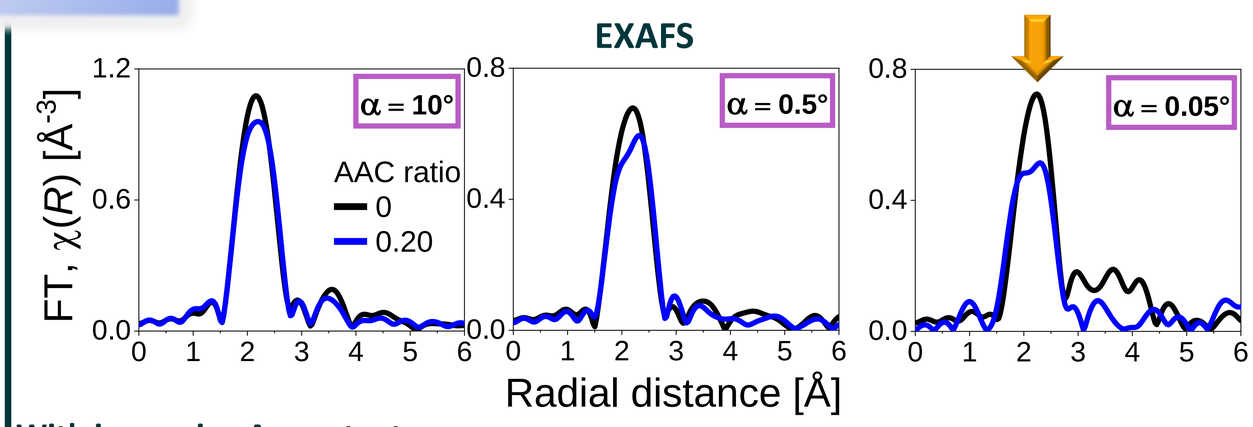

With increasing Ag content:

- Non-linear trend between average Se–[I] and Se–[III] bond lengths with composition
- The anion position in the mixed ACIGS system is influenced by sublattice sharing of Ag and Cu, or In and Ga, thus strongly depends on changes in the composition
- A coexistence of many different anion configurations is expected

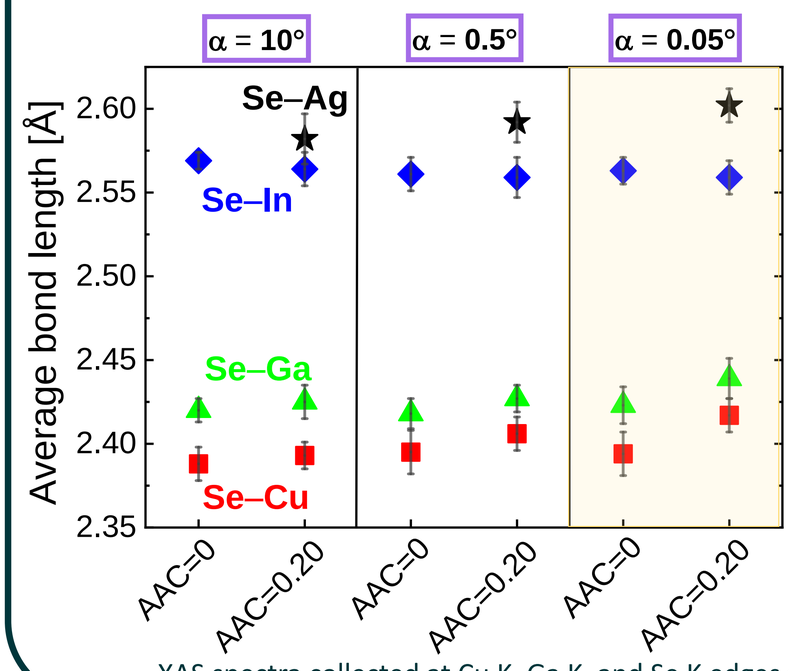

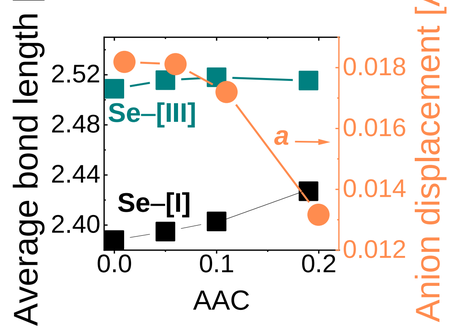

Local vs. crystallographic structure variations within the solar cells

XAS spectra collected at Cu K, Ga K, and Se K edges at room temperature at APS.

Conclusions

- Local atomic arrangement for the investigated ACIGS absorbers is depth-dependent (due to compositional variations) and deviates from the long-range crystallographic structure.
- Investigation of TFCSs at atomic level through synchrotron techniques offers opportunities for rational design of solar cells with improved efficiencies.

References

1. N. M. Martin et al. *ACS Appl. Ener. Mater.* 2022, 5, 461.
2. J. D. Sachs et al. Nat. Sustain. 2019, 2, 805.

Acknowledgements

Argonne NATIONAL LABORATORY
STandUP for ENERGY
Vetenskapsrådet Swedish Research Council

The Role of the Dopant on Electronic Structure of Er-doped Oxides for Quantum Memory

J.B. Martins[1], G. Grant[2,3], K. Sautter[2,3], R. Chebrolu[2], S. Guha[2,3], and J.W. Freeland[1]

[1]X-ray Science Division, Argonne National Laboratory, Lemont, IL 60439
[2]Pritzker School of Molecular Engineering, The University of Chicago, Chicago, IL 60637
[3]Center for Nanoscale Materials, Argonne National Laboratory, Lemont, IL 60439

Rare earth ion defects in solid-state hosts are excellent candidates for applications in quantum communication technologies as qubit systems, due to their inherent spin-photon interface and long coherence times[1]. Er^{3+} is an especially promising candidate due to its $^4I_{15/2} \rightarrow {}^4I_{13/2}$ transition in the telecom C-band. This classically forbidden transition is made accessible by placing Er^{3+} ions within a crystal host, which makes the transition sufficiently bright to use for quantum communication. Oxides are an excellent class of hosts for rare-earth ions due to their straightforward growth even at high purity and expected overall good coherence times when hosting defects[2]. X-ray absorption spectroscopy (XAS) is an element-specific technique broadly applied for local electronic structure characterization in materials. In this work, we performed XAS at the Advanced Photon Source to probe the electronic structure of Er-doped oxides as a function of the doping level. This information is crucial for controlling the tunability of excited state lifetimes and rare-earth defect linewidths in such systems.

[1] Zhong, M. et al. Nature, 2015, 517, 177–180.
[2] Kanai S. et al., arXiv, 2021, 2102.02986.

This material is based upon work supported by the U.S. Department of Energy Office of Science National Quantum Information Science Research Centers as part of the Q-NEXT center.

The Role of the Dopant on Electronic Structure of Erbium-Doped Oxides for Quantum Memory

Jessica Barbosa Martins[1]*, Gregory Grant[2,3], Kathryn Sautter[2,3], Rishi Chebrolu[3], Supratik Guha[2,3], John W. Freeland[1]

[1]*X-ray Science Division, Argonne National Laboratory*
[2]*Materials Science Division, Argonne National Laboratory*
[3]*Pritzker School of Molecular Engineering, University of Chicago*

Introduction

Rare-earth ion defects in solid-state hosts are promising candidates for application as quantum memories and quantum repeaters, due to their inherent spin-photon interface and long coherence times[1]. Er^{3+} ion is especially promising due to its 4f-4f optical $^4I_{15/2} \rightarrow {}^4I_{13/2}$ transition in the telecom C-band, enhanced when it is embedded into a solid host. Oxides are an excellent class of hosts for rare-earth ions due to their straightforward growth and expected overall good coherence times when hosting defects.[2]

The understanding of the electronic structure of these systems are crucial for controlling the tunability of excited state lifetimes and rare-earth defect linewidths. In this work, we performed XANES experiments at the beamline 29-ID-D of the Advanced Photon Source at Argonne National Laboratory. We probed the Ti L– and Er M–edges by XAS from Er:TiO_2 films grown using molecular beam epitaxy (MBE) varying dopant concentrations.

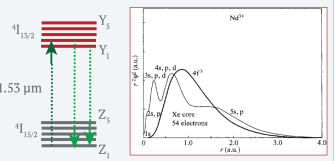

Er^{3+} Optical Transition

Nd^{3+} radial wavefunction.The 4f electrons are shielded by the 5s shell.

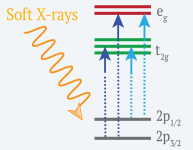

Ti 2p → 3d electronic transition

Experimental Details

The undoped and 200 ppm Er-doped rutile TiO_2 thin films were grown on r-sapphire using molecular beam epitaxy (MBE) by Guha's research group. The edge of r-plane sapphire (1-102) is perpendicular to the sample's a-plane (11-20). The thickness of the thin films are of about 65nm.

We measured the X-ray absorption spectra for the O K-edge, Ti L-edge, and Er M_5-edge on beamline 29 ID-D of the Advanced Photon Source. The spectra were collected in total electron yield (TEY) and fluorescence yield (FY) modes and recorded with the incident X-rays perpendicular and grazing (10°) to the sample surface. The electric field vector (**E**) was aligned either parallel or perpendicular to the *a* axis of the film by flipping the linear polarization of the light from horizontal (H) to vertical (V) polarization. The X-ray Linear Dichroism (XLD) signal was obtained from the difference between V and H polarization spectra.

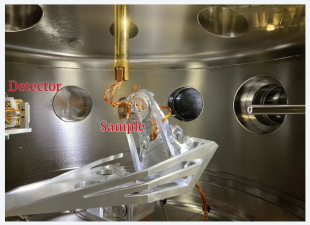

Image of the kappa diffractometer inside the UHV RSXS chamber at the 29ID-D beamline of the Advanced Photon Source.

O K-edge XANES

Normal Incidence

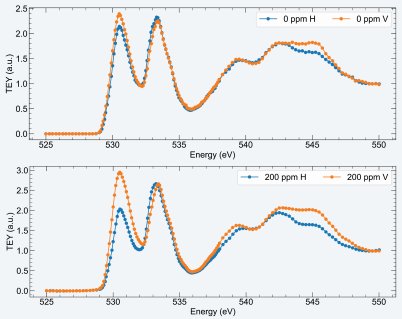

Grazing Incidence

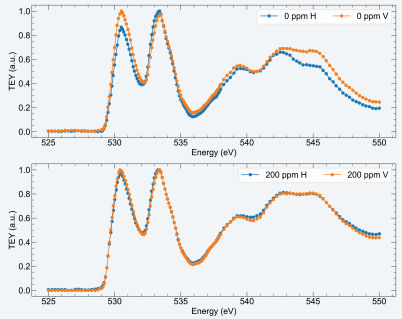

Oxygen K-edge probed by XAS in horizontal (H) and vertical (V) beam polarizations for undoped and 200 ppm Er-doped TiO_2. The presence of the dopant results in strong anisotropy observed from normal incidence measurements.

X-ray Linear Dichroism (XLD)

Normal Incidence

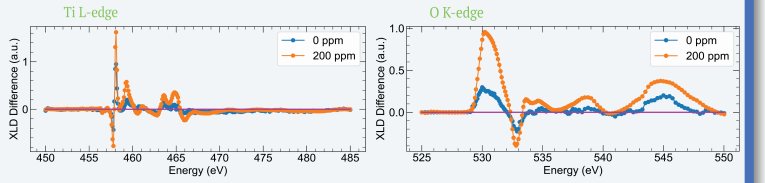

Grazing Incidence

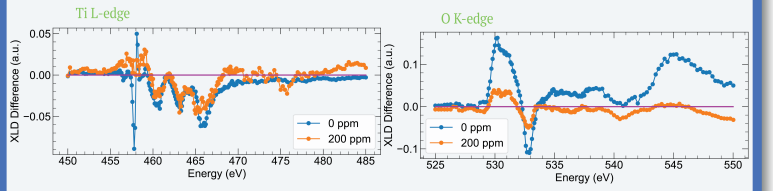

Er M_5-edge

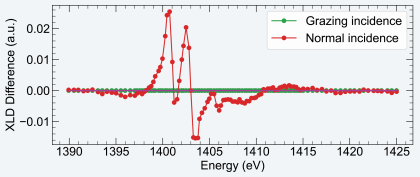

Comparison between XLD signals from measurements at normal and grazing incidence of the beam to the sample surface. Note the weak XLD signal for measurements at grazing incidence and its absence for Erbium. This indicates no out-of-plane anisopropy.

Ti L-Edge XANES

Normal Incidence

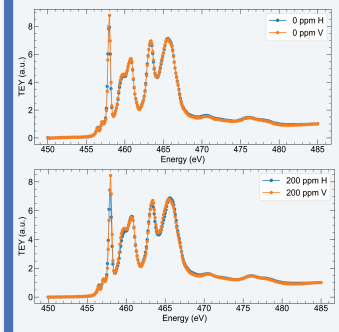

Grazing Incidence

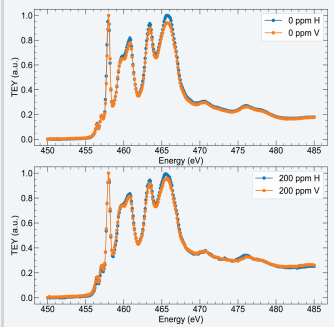

Ti L-edge XAS spectra measured in normal and grazing incidence of the beam in respect to the sample surface. H and V stand for horizontal and vertical polarization of the light.

X-ray Diffraction (XRD)

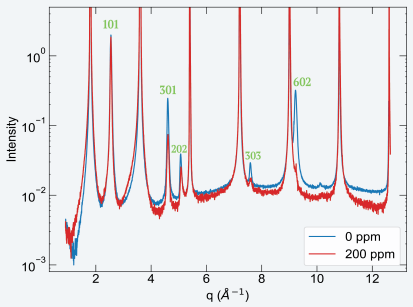

Single crystal X-ray diffraction of (101) rutile TiO_2 samples on the (012) surface of sapphire (Al_2O_3). There is <10% phase with (301) orientation. Both samples are single crystal.

Perspectives

Extended X-ray Fine Structure (EXAFS)

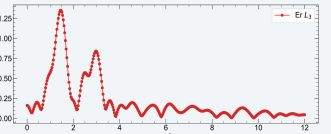

Information on local atomic environment

Fresh data measured at beamline 20-BM of the Advanced Photon Source

Resonant Inelastic Scattering (RIXS)

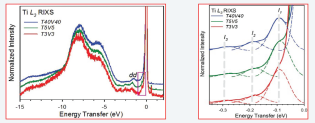

Figures from reference [3].

dd excitations related to Ti^{2+} formation

Er^{3+} interaction with the crystal lattice

Observe changes in phonons: important for coherence

References and Acknowledgements

[1] Zhong, M. et *al.* Nature, 517, 177–180, 2015.

[2] Kanai, S. et *al.*, arXiv, 2102.02986, 2021.

[3] Eres, G. et *al.*, Adv. Func. Mat., 30, (51), 2020.

Argonne NATIONAL LABORATORY
Q-NEXT NEXT GENERATION QUANTUM SCIENCE AND ENGINEERING
THE UNIVERSITY OF CHICAGO
U.S. DEPARTMENT OF ENERGY | Office of Science

In-Situ X-ray Absorption Spectroscopic Characterization of Oxidized Iron Intermediates in the Catalytic Oxidation of CO with N_2O

Jacklyn N. Hall[1], A. Jeremy Kropf[1], Massimiliano Delferro[1], and Praveen Bollini[2]

[1]Chemical Sciences and Engineering Division, Argonne National Laboratory, Lemont, IL 60439
[2]William A. Brookshire Department of Chemical and Biological Engineering, University of Houston, Houston, TX 77204

Elucidating relationships between active site speciation and catalytic function continues to remain a challenge in heterogeneous catalysis, although in-situ studies under reaction-relevant operating conditions can provide novel insight into the nature of active sites and aid in clarifying complex reaction mechanisms. *In-situ* x-ray absorption spectroscopy (XAS) measurements specifically have been widely used in the field of catalysis to reveal information regarding the oxidation state and local coordination environment of active species during reaction that can be key to identifying kinetically-relevant intermediates and determining reactivity-dependent catalyst changes.

Here, we describe for a metal-organic framework (MOF) catalyst, formed by the combination of Fe_3O inorganic nodes linked by organic trimesate molecules, the use of *in-situ* XAS measurements to identify short-lived reaction intermediates key to the redox activity for the reaction of CO with N_2O. Specifically, a microreactor assembly was employed for monitoring the catalyst in a plug-flow design using a capillary polyimide tube for supporting the catalyst to allow sufficient x-ray transmittance at the iron K-edge. Under steady state reaction conditions at 473 K, different equilibrated concentrations of oxidized iron intermediates were identified under varying partial pressures of the reactants. Through estimation of Fe-O bond lengths by analysis of the extended x-ray absorption fine structure combined with linear combination fitting of the absorption edge for characterizing the iron oxidation state, it was determined that the reaction of N_2O with Fe^{2+} active sites results in the formation of iron-oxyl (Fe^{3+}-O^{-}) intermediates. Results of this work provide novel insight into the transitory reactive species, aids in explaining their more radical character in comparison to iron-oxo (Fe^{4+}=O^{2-}) species characterized in other classes of synthetic catalysts,[1] and may be applicable toward understanding structure-activity relationships in heterogeneous catalysts, more broadly.

The authors acknowledge funding through award # 61226-DNI5 from the American Chemical Society Petroleum Research Fund. A portion of this work is supported by the U.S. Department of Energy (DOE), Office of Science, Office of Workforce Development for Teachers and Scientists, Office of Science Graduate Student Research (SCGSR) program under contract number DE-SC0014664. Work at Argonne National Laboratory was supported by the U.S. DOE, Office of Basic Energy Sciences, Division of Chemical Sciences, Geosciences, and Biosciences, Catalysis Science Program under Contract No. DE-AC-02-06CH11357. Use of the Advanced Photon Source is supported by the U.S. DOE, Office of Science, and Office of the Basic Energy Sciences, under Contract No. DEAC02−06CH11357.

[1] Synder, B.E.R., *et al*. *Nature* 536 (2016) 317-321.

In-Situ X-ray Absorption Spectroscopic Characterization of Oxidized Iron Intermediates in the Catalytic Oxidation of CO with N_2O

Jacklyn N., Hall[1,2], A. Jeremy Kropf[1], Massimiliano Delferro[2], and Praveen Bollini[2]*

[1] Chemical Sciences and Engineering Division, Argonne National Laboratory, Lemont, IL 60493

[2] William A. Brookshire Department of Chemical and Biological Engineering, University of Houston, Houston, TX 77204

Background & Motivation

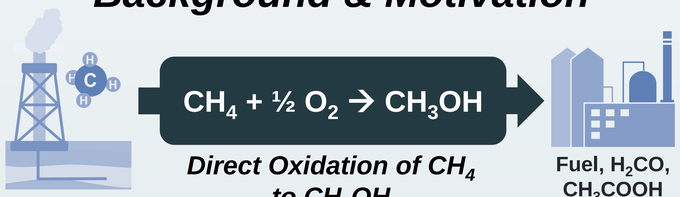

Bio-Inspired Metal-Organic Frameworks (MOFs)

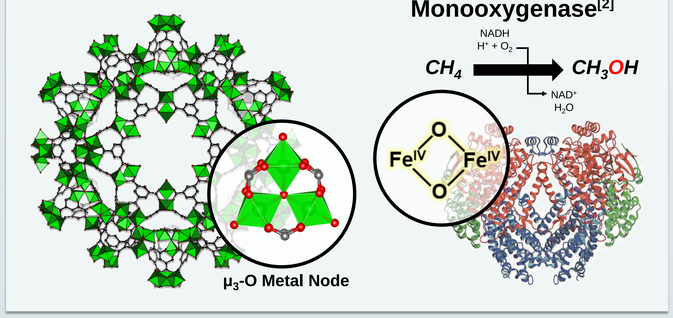

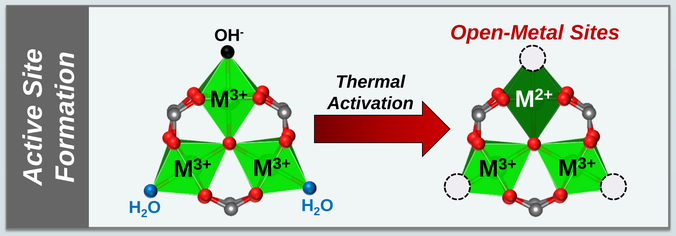

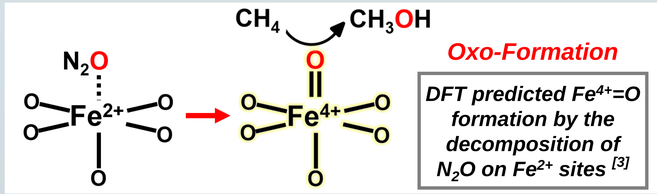

RESEARCH GOAL: Elucidate reaction steps that mediate **redox turnovers over MIL-100(Fe)** with N_2O as an oxidant for the broad purpose of **improving atomic-level efficiencies** for **light alkane conversion**

Acknowledgements

Financial support was provided through award # 61226-DNI5 from the ACS Petroleum Research Fund (PRF). A portion of the work was supported by the U.S. DOE, Office of Science, Office of Workforce Development for Teachers and Scientists, Office of Science Graduate Student Research (SCGSR) program. Work at Argonne National Laboratory was supported by the U.S. DOE, Office of Basic Energy Sciences, Division of Chemical Sciences, Geosciences, and Biosciences, Catalysis Science Program under Contract No. DE-AC-02-06CH11357. Use of the Advanced Photon Source is supported by the U.S. DOE, Office of Science, Office of Basic Energy Sciences, under Contract No. DEAC02-06CH11357.

References

(1) Férey, G., *et al*., *Angew. Chem. Int. Ed*. 43 (2004) 6296. (2) Kopp, D.A., & Lippard, S.J., *Curr. Opin. Chem. Biol*. 6 (2002) 568-576. (3) Vitillo, J.G., et al., *ACS Catal*. 9 (2019) 2870-2879.

Oxidation of CO: Catalytic Probe

CH_4 Oxidation

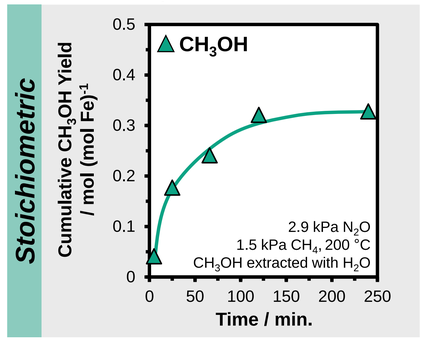

CO Oxidation

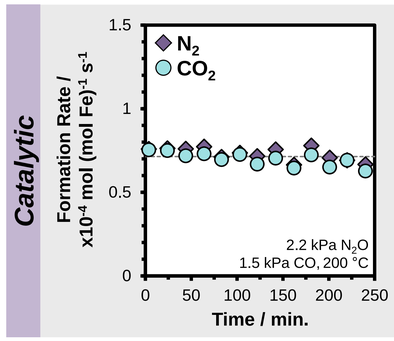

Utilizing catalytic CO oxidation to further understanding of N_2O-mediated redox cycles over trimeric nodes in MIL-100 catalysts

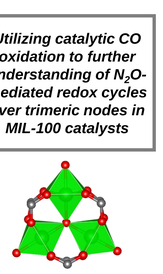

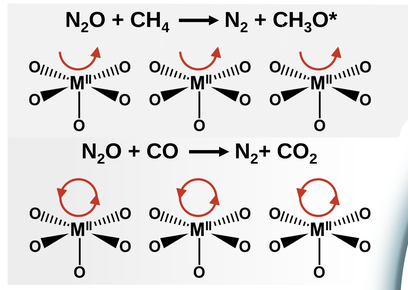

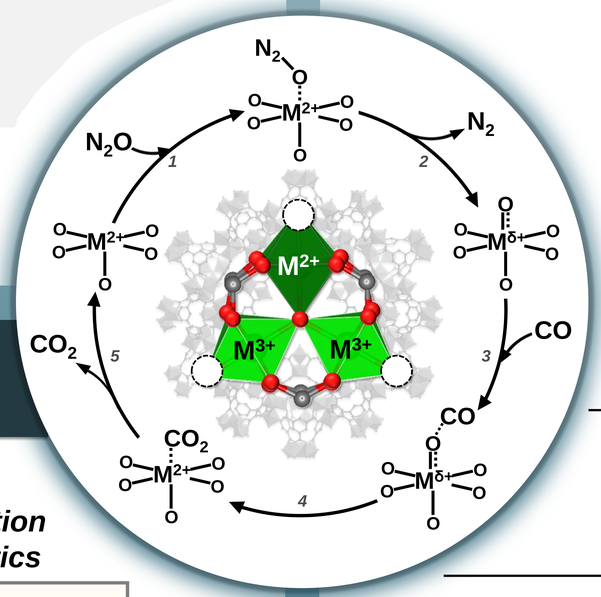

F-O Coverages during Steady-State Reaction

Reaction Kinetics

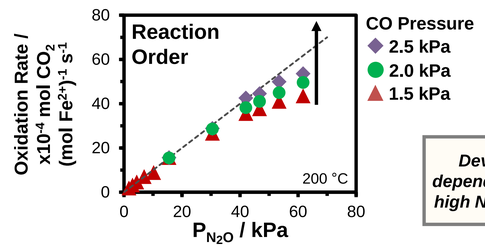

Deviation from first-order dependence on N_2O pressure at high N_2O/CO molar ratios (≥ 20)

Model Fitting

Simplified Rate Expression:

$$r = \frac{k_2K_1[N_2O]}{1 + \left(\frac{k_2K_1[N_2O]}{\overrightarrow{k_3}[CO]}\left(1 - \frac{\overleftarrow{k_3}}{\overleftarrow{k_3} + k_4}\right)\right)[Fe\text{-}O]}$$

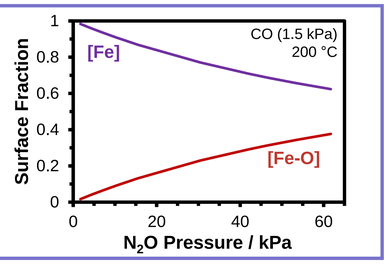

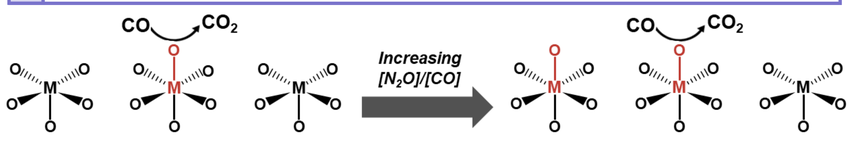

In-Situ XAS Characterization

X-ray Absorption Fine Structure (XAFS) Analysis

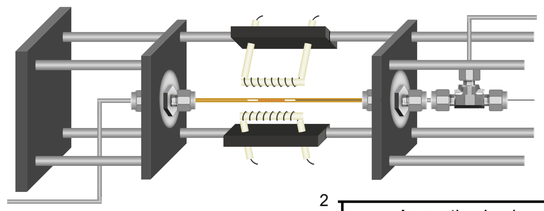

Flow Cell Reactor

Inspired by in-situ XAS cell designs proposed by Chupas et al.
***(J. Appl. Cryst.* 41 (2008) 822)**

Proposed Active Site

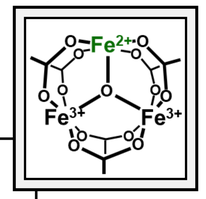

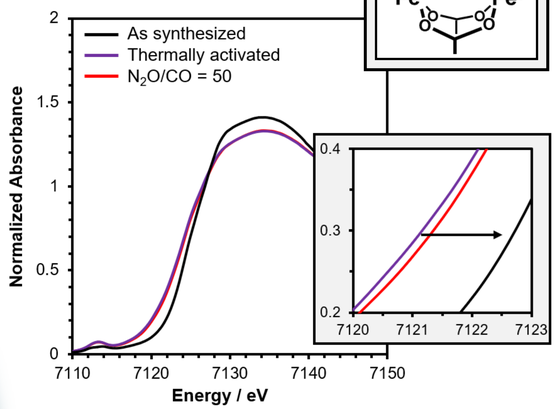

Thermal Activation:
~ 30% of the total iron is reduced from Fe^{3+} to Fe^{2+}

Under Reaction (N_2O/CO = 50):
Oxidation of iron observed in XANES spectra during reaction

Characterizing Fe-O Intermediates

Difference Analysis

Sample Under N_2O/CO - *Thermally Activated Sample* = *Difference Spectra*

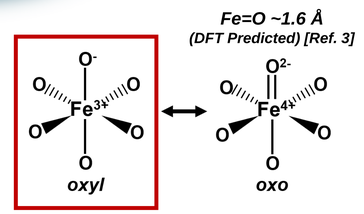

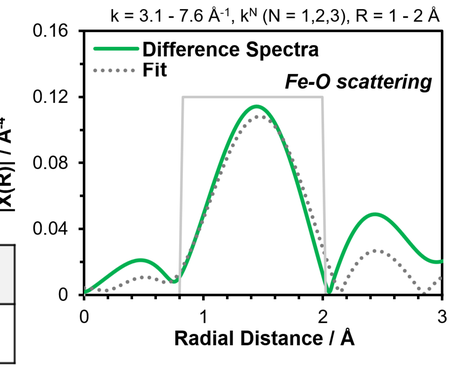

Fe-O Coordination Number	Fe-O Scattering Path Length
0.09 ± 0.03 mol (total mol Fe)$^{-1}$	1.946 ± 0.026 Å

***Fe-O* intermediates exhibit *oxyl character* under steady-state reaction conditions and the fraction of oxidized iron (~ 9%) corresponds closely with estimates from kinetic measurements (~13%)**

Structure and Properties of the Solder Joints Produced in Terrestrial and Microgravity Environment

Manish Kumar[1] and Sid Pathak[1]

Materials Science and Engineering, Iowa State University, Ames, IA 50011

Solder joint porosity is a common but undesirable feature naturally arising from the use of fluxes and is more insidious in soldering joints formed under low-gravity conditions. In the absence of gravity, voids and bubbles are entrapped in the interior of the solder joint upon solidification. The In-Space Soldering Investigation (ISSI) experiments performed aboard the International Space Station (ISS) have shown that soldering in microgravity is expected to be considerably different than their ground-based counterparts due to Earth's natural convective flow and buoyancy effects being minimized in microgravity during melting and solidification. Using Lead-Tin (40wt%Pb-60wt%Sn) solders from the ISSI experiments, along with freshly made terrestrial solders of the same composition, we demonstrate how the lack of Earth's natural convective flow and buoyancy effects during melting/solidification onboard the ISS affects its microstructure and properties in terrestrial vs. microgravity environments. Our scanning electron microscopy (SEM) analysis demonstrate a considerable amount of internal porosity (about four times that of terrestrial solder) in the microgravity solder. High-resolution and high-speed tomography was used to demonstrate the 3-D distribution of pores in microgravity vs. terrestrial solders. Nanomechanical testing demonstrated a corresponding lower strength in the microgravity solders compared to ground-based solders. We also performed a detailed analysis of the substantial effect of aging on the ISSI solder microstructure and properties over the past 17 years. Additionally, we report on the micro-mechanical behavior of the solder joints under extreme conditions of elevated and cryogenic temperatures similar to those typically experienced by the ISS (from +120 C on sun facing side to -150 C on shady side outside the ISS). These tests examine the effects of phase transformation and associated volume and internal stress changes in Sn in Pb-Sn solders during the β-Sn (body-centered tetragonal) to α-Sn (diamond cubic) transformation below 13 C.

Structure and Properties of Pb-Sn Solder joints Produced in Terrestrial vs. Microgravity Environments

Manish Kumar, Dr. Ralph Napolitano, Dr. Sid Pathak*

Materials Science and Engineering, Iowa State University, Ames, IA, USA, 50011

*pathak@iastate.edu

Using Pb-Sn solders from the In-Space Soldering Investigation (ISSI), we demonstrate how the melting and solidification in microgravity onboard the international space station (ISS) are affected by:

- Lack of Earth's natural convective flow
- Dominating forces due to surface tension in the absence of buoyancy
- Thermocapillary flow due to temperature gradient

The microstructure and resultant micro-to-nanomechanical response of solders in terrestrial vs. microgravity environments demonstrate:

- a considerable amount of internal porosity (about twelve times that of ISSI terrestrial solder) in the microgravity solder using SEM analysis.
- lower hardness for microgravity solders than the terrestrial sample which is caused by a coarser grain structure due to long-term aging.
- In-homogeneous microstructure due to thermocapillary flow in ISSI microgravity wire feed solder than ISSI microgravity wire wrap solder.
- In **future** work, we will perform new soldering experiments with controlled soldering parameters onboard the international space station (ISS).
- Micro-mechanical testing under thermal cycling in extreme temperature conditions (from +121 ºC (Sun facing side) to -157 ºC (Shady side)).

Motivation: In-Space Electronics Repair and Metal Joining for Space Missions

- It is important to advance our current electronic and mechanical joint soldering capabilities in space to enable space-based fabrication and repairs.
- Essential for future long-duration human exploration missions beyond low earth orbit (NASA Mars Rover sample return mission and Moons' Artemis program etc.).

Solder prepared in terrestrial conditions	Solder prepared in microgravity conditions
a) – Optical image	b) – Optical image
c) – BSE SEM	d) – BSE SEM
▪ Tear drop shape ▪ Fewer pores	▪ Uniform football shape ▪ More pores

- Results from the In-Space Soldering Investigation (ISSI) experiments performed aboard the International Space Station (ISS) have shown that soldering in microgravity is expected to be considerably different than their ground-based counterparts [1-2].
- Two different methods were used to prepare the solder samples using Near Eutectic 40wt%Pb-60wt%Sn alloy(Kester "44"® 60-40 rosin core solder (3.3 wt.% rosin)

A) Wire wrap solder: Solder wire was wrapped around a silver-plated Cu wire and melted using the soldering iron

B) Wire feed solder: Solder wire was fed onto a silver-plated Cu wire and melted using the soldering iron

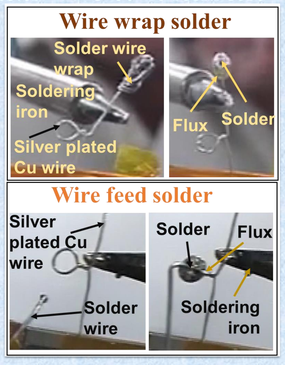

Based on wire wrap solder sample - differences in soldering in microgravity vs. terrestrial conditions:

- Dominating forces due to surface tension – leading to football shape of microgravity solder.
- Lack of buoyancy force and reduced fluid motion in microgravity – Causes increased porosity - affect the mechanical integrity as well as thermal and electrical conductivity.
- The insights gained from this work can be extended to study effects of fluid interfaces with surface tension variations (such as in boiling, heat transfer, welding, brazing, or soldering).

Aging Causes Grain Coarsening and Reduces Hardness (Strength)

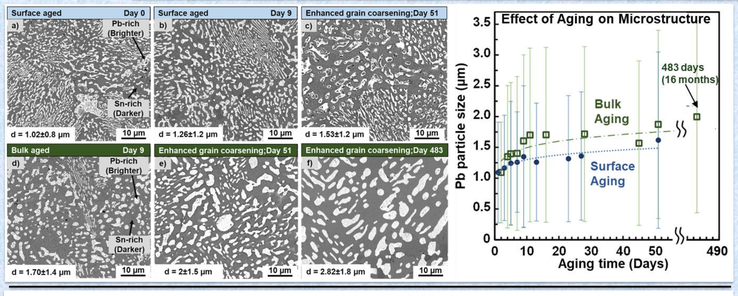

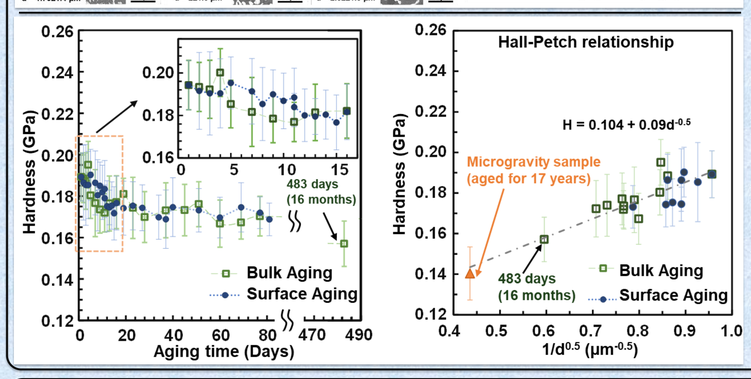

- We studied the aging properties in two different conditions:
  - **Surface aging:** Sample was cut, and same cut surface was examined over the period of the aging study.
  - **Bulk aging:** Intact solder samples were examined

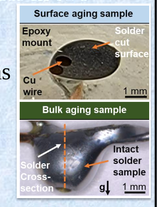

- Increase in Pb particle size in Pb-Sn solder with aging
- Faster aging in bulk conditions than the surface conditions – Probably due to material transport from all directions
- Bulk aging is faster than surface aging – higher curve slope
- Berkovich hardness reduces with aging time due to grain coarsening
- Micrograviy sample demonstrate similar drop in hardness as recently prepared terrestrial solder – it is within the same hardening slope

Hardness variation in ISSI Micrograviy and Terrestrial Solders

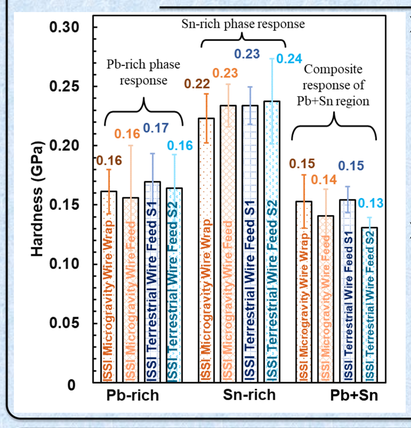

- No significance difference in the hardness of different phases in ISSI micrograviy and ISSI terrestrial solder
- Differences may have been homogenized due to long-term aging

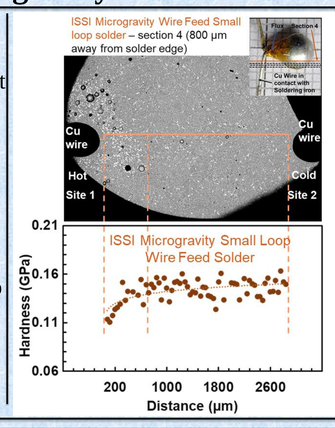

- SEM Image on the left demonstrate the accumulation of voids and Pb-Rich phase - probably due to the thermocapillary flow in ISSI micrograviy wire feed solder
- Lower hardness near Cu wire-1 (in contact with soldering iron) than Cu wire-2 is attributed to the higher amount of softer Pb-Rich phase

Increased Porosity in Micrograviy w.r.t. Terrestrial Solder

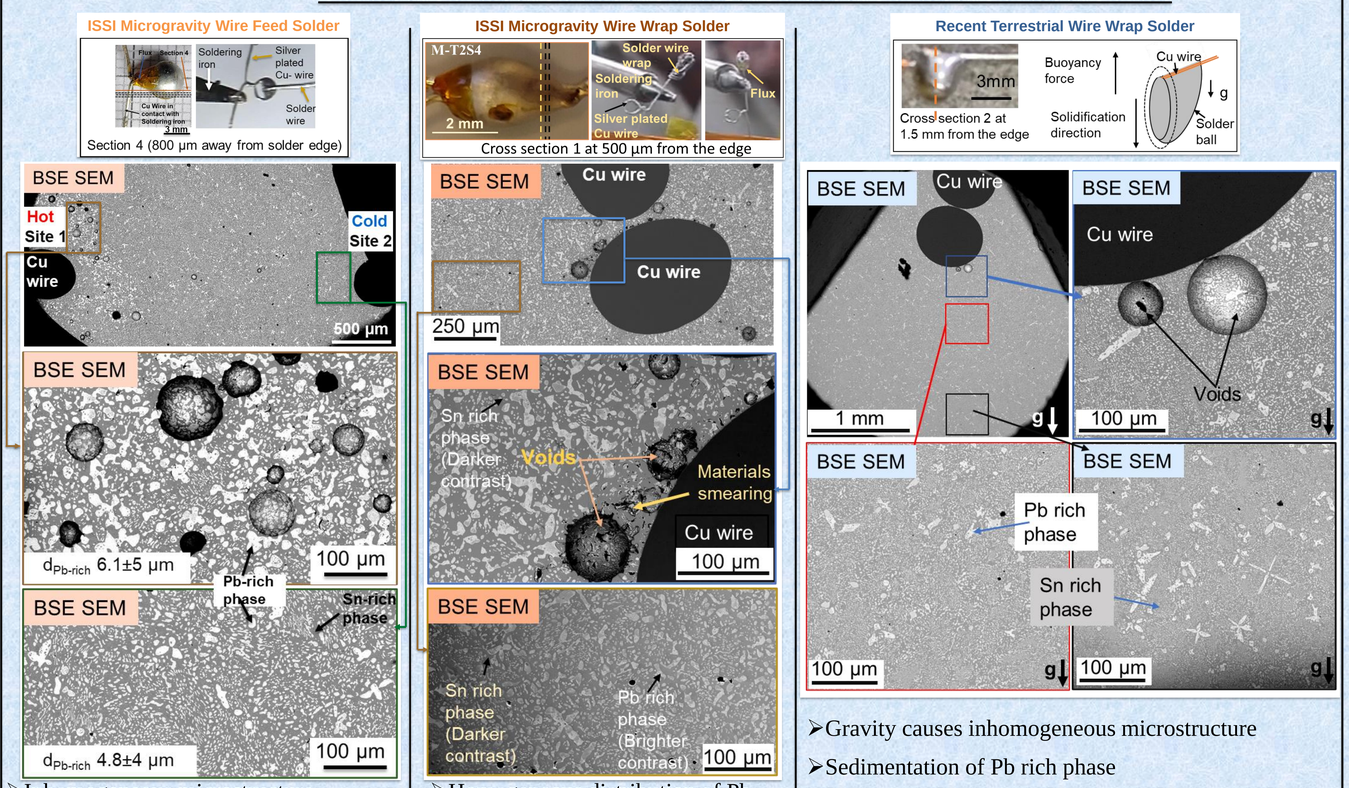

- Inhomogeneous microstructure
- Accumulation of voids and Pb phase - probably due to the thermocapillary flow
- Homogeneous distribution of Pb-rich and Sn-rich phase.
- More voids near the solder joint.
- Gravity causes inhomogeneous microstructure
- Sedimentation of Pb rich phase
- Fewer voids compared to ISSI micrograviy solder.
- Only voids we see are stuck at the Cu wire

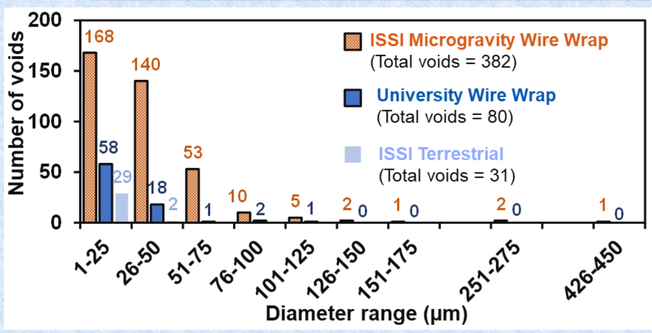

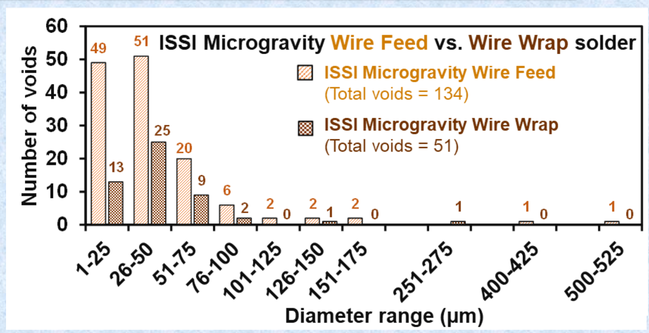

- Higher void volume fraction in micrograviy wire wrap solder than terrestrial wire wrap solder - due to absence of buoyancy force and slower fluid mixing
- Higher void fraction in micrograviy wire feed solder than wire wrap solder
- In wire wrap solder: solder is free to melt around the Cu wire - any flux in the core can exit and remain on the molten solder surface
- In wire feed solder: after a small amount of liquid solder accrues - any flux/rosin from the core is now constrained to remain internal to the liquid

Conclusions:

- Coarser grain structure and reduced hardness due to aging
- Higher fraction of voids in ISSI micrograviy wire feed solder than ISSI micrograviy wire wrap solder – probably attributed to the higher amount of trapped flux in feed solder

Ongoing Work:

- 3-D destructive serial cross-sectioning on remaining ISSI solders sample
- The ISS experiences severe thermal cycling due to switch from +121 ºC (Sun facing side) to -157 ºC (Shady side). Therefore, it is important to investigate solder joint behavior under thermal cyclic loading which can lead to:
  - Accelerated aging at elevated temperature
  - Phase transformation in Sn - Body Centered Tetragonal (BCT) β-Sn to Diamond Cubic (DC) α-Sn (Tin pest) below 13ºC → 27 % volume increase associated with phase transformation

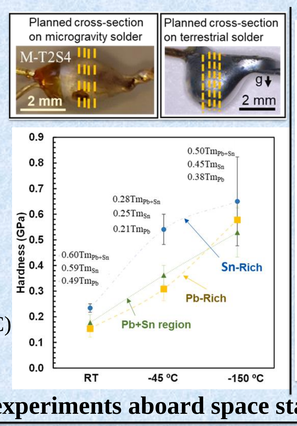

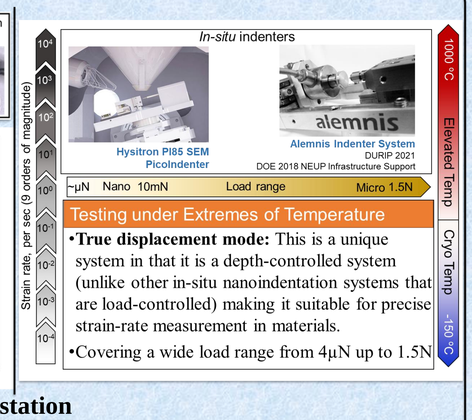

ISS Flight Opportunity: New soldering experiments aboard space station

- We are planning new micrograviy experiments in Fall 2023, which will allow better control of following soldering parameters:

a) Solder composition
- Near eutectic 40Pb-60Sn solders
- Off-eutectic 50Pb-50Sn solders
- Eutectic Sn-Ag-Cu solders

b) Two solder sample design are considered
- Reflow Spreading Specimen (RSS)
- Reflow Filling Specimen (RFS)

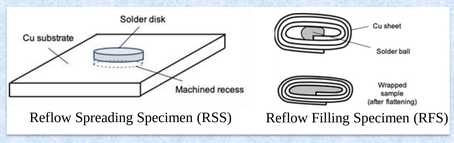

c) Precise control of solder thermal profile such as temperature, heating and cooling rates, hold time at maximum temperature

- Due to higher attenuation from Pb, larger can not be analyzed using non-destructive tomography
- Non-destructive tomography was performed to figure out the sample dimension of the micrograviy solder that we can analyze at the APS

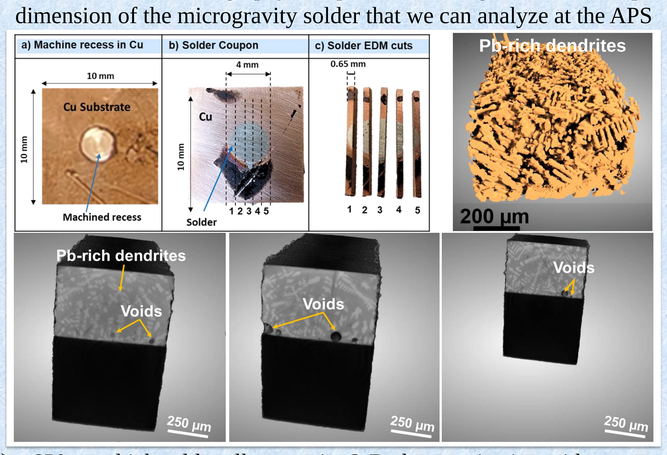

- 650 μm thick solder allows entire 3-D characterization without destructive serial cross-sectioning
- These sample designs can also be used for the potential parabolic flight experiments – Sample size needs to be small in-order to solidify within the short micrograviy duration (18 sec)

Acknowledgement:
Scott Gilley, Tec-Masters, Inc, Huntsville, Al 35806
Jacob Scoccimerra, Nanorack, Houston, TX 77598
NASA EPSCoR **(#80NSSC21M0229)**

Acknowledgements

IOWA STATE UNIVERSITY NASA

NASA Physical Sciences Informatics (PSI) grant
(#80NSSC20K0223 - FY2020)
(#80NSSC23K0279 - FY2023)
NASA EPSCoR **(#80NSSC21M0229)**

Dr. Richard Grugel (NASA scientist, NASA Marshall Space Flight Center)
Dr. Louise Strutzenberg (NASA scientist, NASA Marshall Space Flight Center)
Dr. Binayak Panda (NASA scientist, NASA Marshall Space Flight Center)

References:

1. R. Grugel *et al.*, "Final Research Report. In-Space Soldering Investigation (ISSI)," 2006.
2. M. Struk and R. D. Pettegrew, "Soldering in Reduced Gravity Experiment," *SDTO 17003-U (SoRGE)*, 2017.

Depth Dependent Understanding of Interfacial Properties on the Layered Cathodes at Extreme High Temperature Operation for Nonflammable Li-ion Batteries

Sudhan Nagarajan[1], Conan Weiland[2], Cherno Jaye[2], Sooyeon Hwang[3], Debora Motta Meira[4 $], Mahalingam Balasubramanian[4,5], Leela Mohana Reddy Arava[1]*

[1]Department of Mechanical Engineering, Wayne State University, Detroit, MI 48202
[2]Material Measurement Laboratory, National Institute of Standards and Technology, Gaithersburg, MD 20899
[3]Center for Functional Nanomaterials, Brookhaven National Laboratory, Upton, NY 11973
[4]X-ray Science Division, Advanced Photon Source, Argonne National Laboratory, Lemont, IL 60439
[5]Electrification and Energy Infrastructure Division, Oak Ridge National Laboratory, Oak Ridge, TN 37830

With the current Li-ion battery technology, the batteries can be operated between room temperature and slightly above room temperature(< 55 ^{o}C), and operation beyond this suggested temperature range will lead to irreversible degradation often resulting in low cell capacity, cycle life, and sometimes catastrophic failures such as fires and explosions. However, several industrial applications require high-performance rechargeable batteries operated in aggressive environments such as military applications, sensor applications, and downhole drilling applications.[1] Fundamentally, the high-temperature operation of Li-ion batteries is highly dependent on the stability of the electrode and electrolyte interface during lithiation/delithiation electrochemical reactions (charge/discharge). However, current knowledge on the nature of cathode electrolyte interphase (CEI) formed on cathodes is limited, and its stability under extreme temperature is not well understood. With this motivation, in this work, a proof-of-concept study for stabilizing the CEI formed on model $LiNi_xMn_yCo_zO_2$ (NMC/x+y+z=1) cathode is extensively studied. An in-depth investigation into reversible lithiation/delithiation at extremely high temperature (> 80 ^{o}C) operation in ionic liquid electrolyte combination is evaluated.[2] Further, the depth-dependent interfacial properties of the CEI formed on the NMC cathodes cycled at high temperatures is understood using energy-tunable hard x-ray photoelectron spectroscopy (HAXPES). In addition, the bulk and surface electronic structure evolution at extreme temperature is probed using soft and hard x-ray absorption spectroscopy investigations. Stabilization of the reactive NMC cathode surface at extremely high temperatures using conformal surface passivation and layer-to-spinel structural transformations is visualized using high-resolution transmission electron microscopy (HRTEM) investigations. In this study, understanding the high-temperature interfacial stability of the NMC cathode materials through multimodal spectroscopy and microscopy is focused to transform the ambient temperature Li-ion battery technology to extreme temperature applications.

[1] Lin, X.; Salari, M.; Arava, L. M. R.; Ajayan, P. M.; Grinstaff, M. W., High temperature electrical energy storage: advances, challenges, and frontiers. *Chemical Society Reviews* 2016, *45* (21), 5848-5887.
[2] Nagarajan, S.; Weiland, C.; Hwang, S.; Balasubramanian, M.; Arava, L. M. R., Depth-Dependent Understanding of Cathode Electrolyte Interphase (CEI) on the Layered Li-Ion

Cathodes Operated at Extreme High Temperature. *Chemistry of Materials* 2022, *34* (10), 4587-4601.

This material is based upon work supported by the National Science Foundation under grant number 1751472. We also acknowledge funding support from the Advanced Energy Consortium (AEC) (BEG14-02). http://www.beg.utexas.edu/aec/partners companies include BHP, ExxonMobil, US Department of Energy, Repsol, Sandia National labs, and Total. This research used resources of the National Synchrotron Light Source II (NSLS-II); a U.S. Department of Energy (DOE) Office of Science User Facility operated for the DOE Office of Science by Brookhaven National Laboratory under Contract DE-SC0012704. The NEXAFS and HAXPES measurements were performed at the National Institute of Standards and Technology (NIST) beamlines SST-1 and SST-2 in the NSLS-II, respectively. This research also used resources of the Center for Functional Nanomaterials, which is a U.S. DOE Office of Science Facility, at Brookhaven National Laboratory under Contract No. DE-SC0012704. This research used resources of the Advanced Photon Source (APS); an Office of Science User Facility operated for the U.S. Department of Energy (DOE) Office of Science by Argonne National Laboratory under Contract No. DE-AC02-06CH11357.

Depth Dependent Understanding of Interfacial Properties on the Layered Cathodes at Extreme High Temperature Operation for Nonflammable Li-ion batteries

Sudhan Nagarajan[1], Conan Weiland[2], Cherno jaye[2], Sooyeon Hwang[3], Debora Motta Meira[4], Mahalingam Balasubramanian[4 #], Leela Mohana Reddy Arava[1 *]

[1]Department of Mechanical Engineering, Wayne State University, Detroit, MI,48202, * leela.arava@wayne.edu
[2]National Synchrotron Light Source-II, [3]Center for Functional Nanomaterials, Brookhaven National Laboratory,
[4]Advanced Photon Source, Argonne National Laboratory , # present address : Oak Ridge National Lab

2023 APS/CNM Users' Meeting, April 17-21 , 2023

Introduction

With the current Li-ion technology, the batteries can be operated between room temperature to ~60°C, and operation beyond this suggested temperature range will lead to irreversible degradation often resulting in low cell capacity, cycle life, and sometimes catastrophic failures such as fires and explosions. However, several industrial applications require high-performance rechargeable batteries operated in aggressive environments such as military, sensor, and downhole drilling applications. (1) Fundamentally, the high-temperature operation of Li-ion batteries is highly dependent on the stability of electrode and electrolyte interface during lithiation and delithiation reactions. However, knowledge on the nature of cathode electrode interphase (CEI) formed on cathodes is limited and its stability under extreme temperatures is not well understood. Therefore, herein, a proof-of-concept study on stabilizing CEI formed on model LiNixMnyCozO2 (NMC/x+y+z=1) cathodes is presented, and an investigation into reversible lithiation/delithiation at extreme high temperature (100°C) operation in ionic liquid (IL) electrolyte combination with film-forming additives is evaluated. (2) In this study, understanding the high-temperature interfacial stability of NMC cathode materials through advanced spectroscopy and microscopy will shed light on transforming ambient temperature technology into high-temperature applications.

Methodology

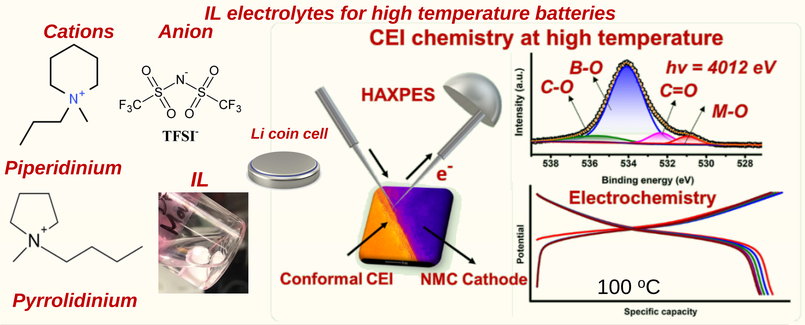

Electrochemistry Investigation

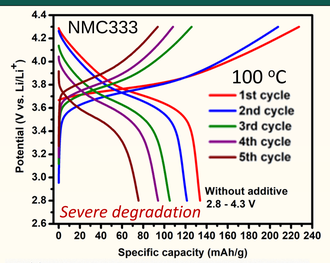

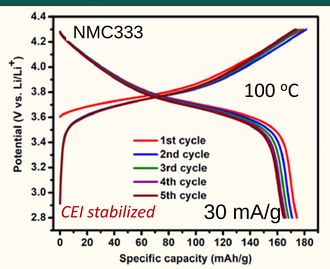

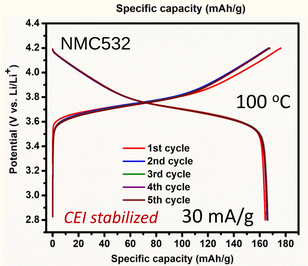

- The electrochemical analysis of NMC33 cathode in pyrrolidinium (Py) based ionic liquid at 100 °C exhibited poor lithiation/delithiation properties due to parasitic reaction between NMC333 cathode and ionic liquid electrolyte.
- CEI stabilization improved the reversibility at high temperature operation for both NMC333 and NMC532 compositions

Hard and Soft X-ray Absorption Spectroscopy study

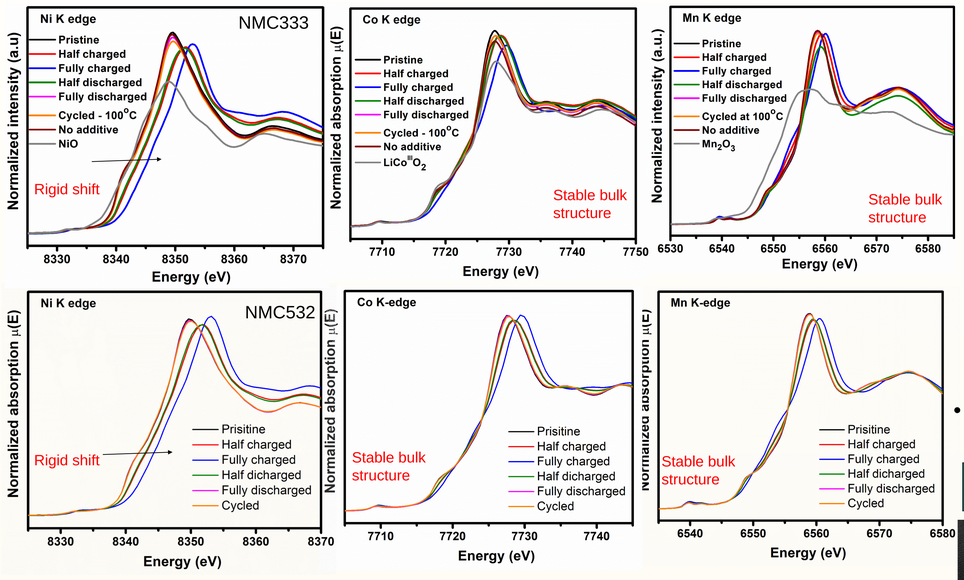

- Bulk sensitive transmission mode X-ray Absorption spectroscopy investigation of NMC cathodes cycled at high temperature.
- Rigid shift in absorption edge clearly evidenced the oxidation state changes- Ni^{2+} to Ni^{4+}
- Co and Mn K-edge exhibit no rigid shift to high energy during high temperature electrochemical reaction. If bulk electronic structure is stable, – What is the origin of degradation?

Surface electronic structure study

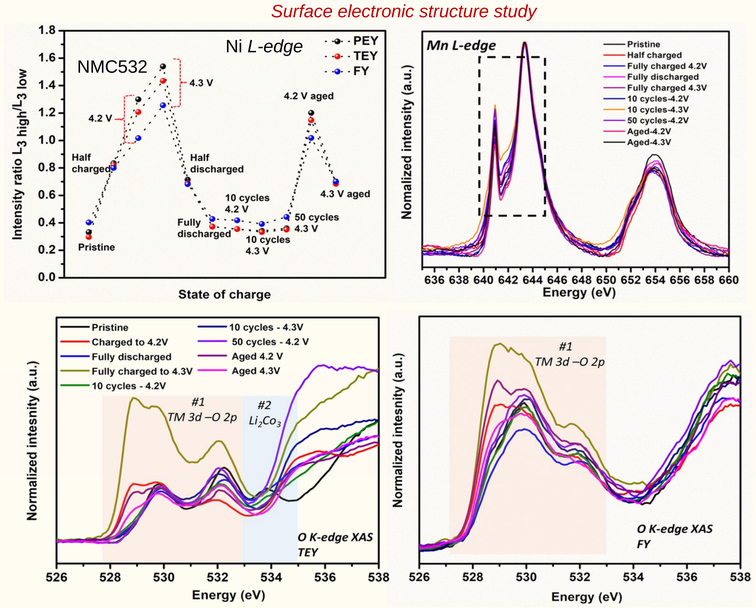

- Probing depth : PEY- 1 nm to 2 nm, TEY ~5 nm, FY ~50 nm to 100 nm.

- The sXAS is certainly helpful to understand depth dependent transition metal evolutions.
- The metal L edge spectra provide information from peak shifts, shapes and intensity ratios.
- Intensity ratios clearly evidence the valence state heterogeneity at different depth level for Ni L-edge. The observed Mn L edge peak shapes have changed due to slight valence state variation.
- Oxygen K edge measurement was done at both surface (TEY) and bulk (FY) detection modes. Area under the curve conveys a lot about metal- ligand covalency that is mainly originated from transition metal and oxygen ligand.
- Though ionic liquids are thermally stable, electrode and electrolyte interface is not stable.

Hard-X-ray Photoelectron Spectroscopy study

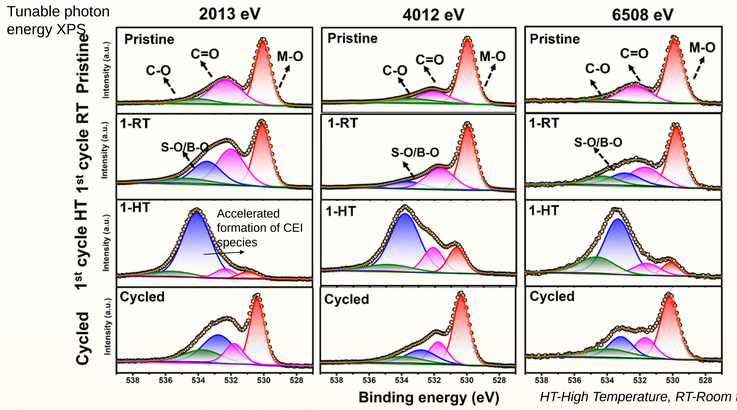

HT-High Temperature, RT-Room temperature

- Depth dependent O 1s HAXPES spectra of NMC333 cathode materials cycled at different conditions. Surface passivation is accelerated at high temperature

High-resolution Transmission Electron Microscopy

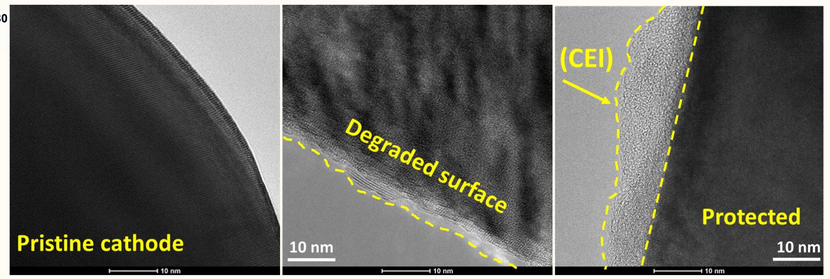

- HRTEM image visualized the CEI formation on the NMC cathode surface.
- Unprotected cathode exhibits severe surface degradation.

Key conclusions

- According to this obtained capacity (~175 mA/g at 30 mA/g), the extraction ratio is ~62% at 100 °C, indicating the capacity contribution at extreme temperature is purely from Ni redox center and not from parasitic reactions .
- The conformal CEI formation on a cathode surface is accelerated during initial cycles at high temperature compared to room temperature.
- Depth dependent electronic structure heterogeneity is the fundamental reason for degradation. (NMC532)
- Conformal passivation ability on the NMC cathode surface was visualized with HRTEM investigation, unveiling that the CEI protects the reactive surface from electrolyte attack at extreme temperature.

References

1. Lin, X.; Salari, M.; Arava, L. M. R.; Ajayan, P. M.; Grinstaff, M. W. Chemical Society Reviews 45, 5848-5887 (2016)
2. Nagarajan, S.; Weiland, C.; Hwang, S.; Balasubramanian, M.; Arava, L. M. R. Chemistry of Materials 34, 4587-4601 (2022).

Acknowledgement

This research primarily used the resources of Advanced Photon Source beamline 20-BM, Argonne, Brookhaven National Lab facilities in Center for Functional Nanomaterials, and NIST beamlines SST-1 and SST-2 in the National Synchrotron Light Source-II.

Modulating Assemblies of Amphiphiles and Nanoparticles via Solution Ionic Environment

Roger J. Reinertsen[1*], Joseph M. McCourt[2*], Sumit Kewalramani[1], Monica Olvera de la Cruz[1, 2, 3], and Michael J. Bedzyk[1, 2]

[1]Department of Materials Science and Engineering, Northwestern University, Evanston, IL 60208
[2]Department of Physics and Astronomy, Northwestern University, Evanston, IL 60208
[3]Department of Chemistry, Northwestern University, Evanston, IL 60208

Charged molecular and colloidal objects in solutions are ubiquitous in nature, and their assembly into nanoscopic superstructures is not only technically useful, but also enables the existence of life itself. The effective charges of molecular or colloidal components, as well as the nature and range of the interactions between them, are coupled to the ionic environment of the solution. In the interest of elucidating the nature of this coupling, we utilize two model systems to investigate charge-controlled-nanoscopic structure via SAXS-WAXS studies at Sector 5 and 12 of the APS.

In the first system, we investigate the assemblies of a charged chiral amphiphilic molecule. For our system, crystalline flat bilayer nanoribbons convert to helical ribbons when the electrostatic interactions are weak, but long-ranged. By contrast, for short-ranged electrostatic interactions, we find helicoidal scrolls (cochleates). In the second system, which consists of non-base-pairing DNA-functionalized gold nanoparticles, we have demonstrated that divalent cations can assemble the particles into colloidal crystals with different symmetries and degrees of ordering; these assemblies continue to evolve with solution salt concentration even at the highest salt concentrations, where classical theory predicts electrostatic interactions to be of negligible range.

In Situ X-ray Scattering Studies of Charged Amphiphile and Nanoparticle Assemblies

Roger J. Reinertsen, Joseph M. McCourt, Changrui Gao, Sumit Kewalramani, Michael J. Bedzyk
Northwestern University, Evanston, IL-60208
NU Theory Collaborators: F. Jiménez-Ángeles, D. Valencia and M. Olvera de la Cruz
DND Collaborators: S. Weigand Sector 12 Collaborators: S. Seifert

Abstract: Charged molecules and colloidal particles in solutions are ubiquitous in nature, and their assembly into nanoscopic superstructures is not only technically useful, but also enables the existence of life itself. The effective charges of molecular or colloidal components, as well as the nature and range of the interactions between them, are coupled to the solution ionic environment. In the interest of elucidating the nature of this coupling, we utilize two model systems to investigate charge-controlled-nanoscopic structure via SAXS-WAXS studies. (1) We investigate the assemblies of a charged chiral amphiphilic molecule. For our system, crystalline flat bilayer nanoribbons convert to helical ribbons when the electrostatic interactions are weak, but long-ranged. By contrast, for short-ranged electrostatic interactions, we find helicoidal scrolls (cochleates).
(2) We investigate how salt concentration modulates the assembly of non-base-pairing DNA-functionalized gold nanoparticles into colloidal crystals with different structures.

Experimental set-up: The measurements were performed primarily using the SAXS/WAXS detector set-up, along with the capillary flow cell at beamline **5ID-D** and beamline **12ID-C** at the Advanced Photon Source (APS) at Argonne National Lab.

Interparticle Interactions in Concentrated Electrolytes

Dissolved ions act as mediators of electrostatic forces in aqueous systems. Beyond simple attenuation (screening) of such forces, ions can also induce more exotic behavior such as attractions between like charges. Additionally, in highly concentrated electrolytes, surprising behavior has been observed, such as an increase of the effective range of electrostatic interactions (the Debye Length) with ionic concentration.

Approach: Small angle X-ray scattering (SAXS) is utilized to investigate the crystal symmetries and effective particle separations of DNA-functionalized gold nanoparticles assembled in concentrated solutions of divalent salts. The DNA is a non-base - pairing (35 base) single-stranded oligonucleotide coupled via a thiol linkage to a 10nm AuNP core.

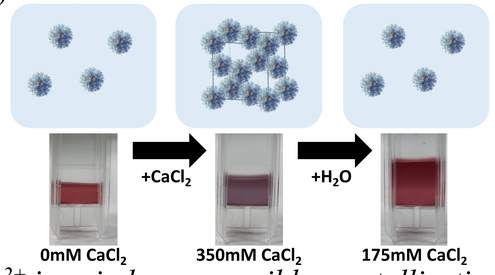

Ca^{2+} ions induce reversible crystallization

Face-Centered Cubic (FCC) **Body-Centered Cubic (BCC)** **Random-Close Packed (RCP)**

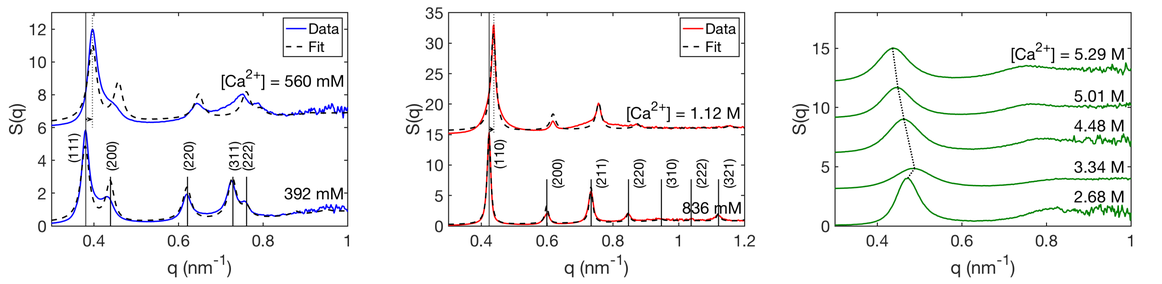

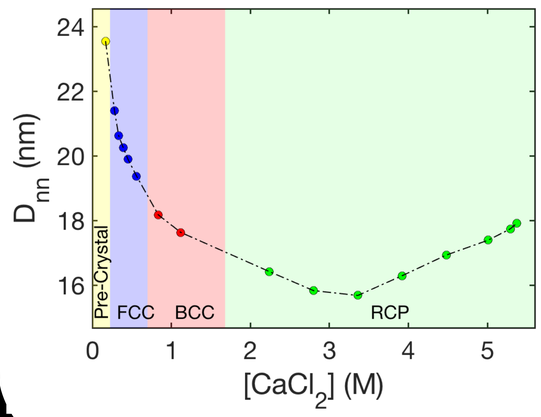

Ion-Driven Behavior:

- Increasing the concentration of $CaCl_2$ changes the lattice type from FCC to BCC to RCP (No long-range order).
- The nearest-neighbor distance within the assemblies initially decreases with salt concentration (as expected), but eventually reaches a minimum and begins to increase. This qualitatively corroborates an anomalous increase in screening length in a nanoscale system. This originates from bulk ionic correlations as seen by WAXS.

Electrostatic control of assembly of chiral amphiphiles

Charged chiral molecules are abundant in nature. Prime examples are amino acids. Efficient packing of chiral molecules requires that the neighbors exhibit a twist with respect to each other, leading to mesoscopic helical structures. Here, we show that the nature of the ionic environment determines the type of helical assembly, with weak, long-range electrostatic interactions leading to helical ribbons and short-range leading to cochleates.

Chiral amphiphile: C_n-Lysine

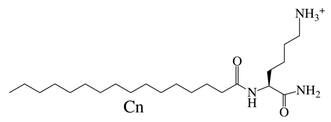

Approach. The assembly of charged chiral amphiphile C_n-K_1 is examined as a function of NaCl and NaOH concentration from nano-to-meso-scale using a combination of in situ AFM, cryo-TEM, circular dichroism and solution SAXS/WAXS.

AFM/Theory

Assembly: Added NaOH

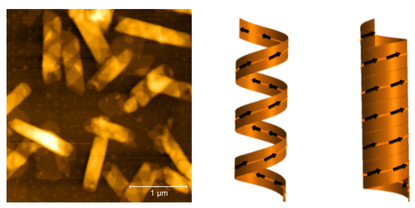

$$NH_3^+ + OH^- \overset{K_a}{\rightleftharpoons} NH_2 + H_2O$$

Assembly: Added salt

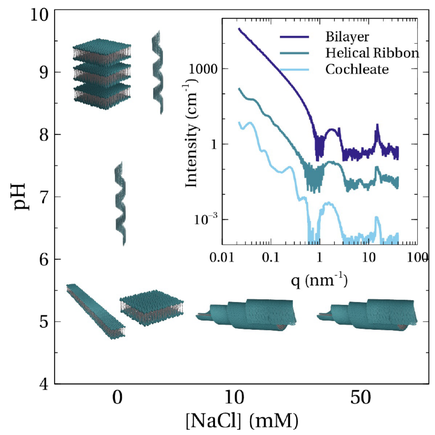

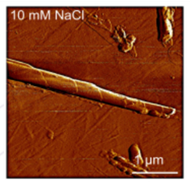

$$V(r) \sim e^{-r/\lambda_D} \qquad \lambda_D \sim \frac{1}{\sqrt{[NaCl]}}$$

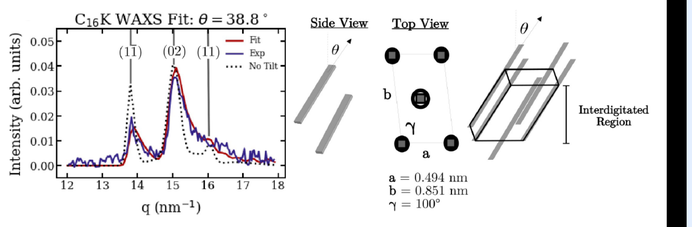

The molecules assemble into planar, interdigitated, high-aspect ratio, tilted, crystalline bilayer ribbons. With a change in ionic environment, the crystallinity in bilayers reduces and bilayers twist. Depending on whether the change tunes the charge (added NaOH (increased pH)) or screens the charge (added NaCl), the bilayer ribbons form helical ribbons or helicoidal cochleate. The phase the diagram above shows the case for $C_{16}K_1$ (n=16).

Generality of Transitions

- The flat bilayer ribbon to helical ribbon transition is general for different hydrophobic tail lengths and membrane rigidities (n=12, 14, 16).
- Membrane rolling is driven by an interplay between the electrostatics and elasticity, which includes contributions due to molecular chirality and tilt.
- The membrane folding direction is determined by the chirality of the constituent molecules, as determined through circular dichroism.

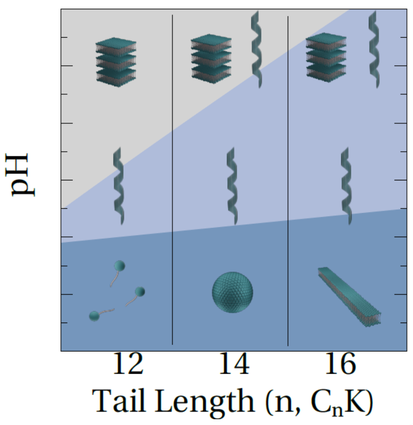

Acknowledgements

- Colloidal assembly: Department of Energy, Basic Energy Sciences (BES): DE-SC001893
- Molecular assembly: Department of Energy, BES: DE-FG02-08ER46539.
- The use of APS is supported by DOE under contract number: DEAC02-06CH11357

X-ray Spectroscopy Measurements on Transverse Thermoelectric Material $CsBi_4Te_6$

Juncen Li[1], Lawrence Rhoads[1], Jessica McChesney[2], Mercouri Kanatzidis[3], and Matthew Grayson[1]

[1]Department of Electrical and Computer Engineering, Northwestern University, Evanston, IL 60208
[2]Advanced Photon Source, Argonne National Laboratory, Lemont, IL 60439
[3]Department of Chemistry, Northwestern University, Evanston, IL 60208

$CsBi_4Te_6$ was first discovered as an excellent low-temperature thermoelectric material when *p*-doped and was soon found to have a highly anisotropic ambipolar Seebeck coefficient when undoped.[1, 2] Such anisotropy makes it an excellent candidate for $p \times n$ transverse thermoelectric materials, which have great potential for solid state cryogenic cooling.[3] Since $p \times n$ materials are a fairly recent discovery, only a handful of such materials have been identified, and none have been examined with x-ray spectroscopy. We performed a suite of soft x-ray spectroscopy measurements such as XPS, resonant XPS, and XAS to probe the structure of single crystal $CsBi_4Te_6$ samples. We confirmed consistency between samples grown from different batches. We used XPS performed at the Cs, Bi, and Te edges to characterize the corresponding oxidation states, and found the oxidation states to be consistent with its chemical composition. We determined there was no polarization dependence. Further XAS and resonant XPS measurements are underway. Results from ongoing attempts to characterize the electronic band structure via ARPES measurements will be presented as well.

[1] Chung, Duck-Young, *et al*. J. Am. Chem. Soc. 2004, 120, 20, 6414-6428.
[2] Chung, Duck-Young, *et al*. MRS Online Proceedings Library (OPL), 2003, 793.
[3] Zhou, Chuanle, *et al*. Phys. Rev. Lett. 2013, 110, 22, 227701.

Light-controlled Spin Coupling in Doped Hybrid Perovskites

Tao Xu[1]

[1]Department of Chemistry and Biochemistry, Northern Illinois University,
DeKalb, IL 60115

The fundamental understanding of spin-involved light-matter interaction can render a potential optic platform for spintronics and spin-based quantum computing. I will present a set of intriguing light-controlled interaction between exciton and localized spin in doped organic-inorganic hybrid perovskites provides. We show that at cryogenic temperature, the spin impurity dopants and the light-induced photocarriers exhibits strong spin coupling via exchange interaction, an optical analogue in semiconductor to Kondo effect in metals.

Light-induced Kondo-like exciton-spin coupling in neodymium(II) doped hybrid perovskites

Xudong Xiao,[1] Jue Gong,[1] Mengyuan Li,[1] Benjamin T. Diroll,[2] Taewoo Kim,[3] Justin G. Connell,[3] Yuzi Liu,[2] H. Christopher Fry,[2] Owen S. Wostoupal,[1] Zhenzhen Yang,[4] Richard D. Schaller,[2] Tao Xu[1*]

[1]*Department of Chemistry and Biochemistry, Northern Illinois University, DeKalb, IL 60115, USA*
[2]*Center for Nanoscale Materials, Argonne National Laboratory, Lemont, IL 60439, USA*
[3]*Material Science Division, Argonne National Laboratory, Lemont, IL 60439, USA*
[4]*Chemical Sciences and Engineering, Argonne National Laboratory, Lemont, IL 60439, USA*

Introduction/Overview

Kondo effect describes the exchange interaction between the localized quantum spin impurity and a large surrounding reservoir of delocalized conduction electrons in metals. The Kondo interaction provides a potential optic platform for light-controlled spintronics and spin-based quantum computing.

Herein, we developed a method to synthesize neodymium(II) doped methylammonium lead triiodide ($MAPbI_3$), demonstrating the interplay between exciton recombination and its Kondo-like interaction with the localized 4f spin impurity.

The characteristic of neodymium(II) doped $MAPbI_3$ was studied and no tremendous change in the crystal structure compared with the pristine $MAPbI_3$. Radiative recombination soars up as evidenced in temperature-dependent steady-state photoluminescence (ss-PL). Notably, the photoelectrons and photoinduced holes, when respectively coupled with 4f spins in antiferromagnetic configuration, recombine at markedly retarded kinetics observed by temperature-dependent time-resolved PL (tr-PL). Further varying the ratio of neodymium(II) dopant concentration to incident photon flux allows modulating the population of Kondo-like coupling.

Temperature-dependent photoluminescence characteristics of pristine $MAPbI_3$ and 2%Nd:$MAPbI_3$

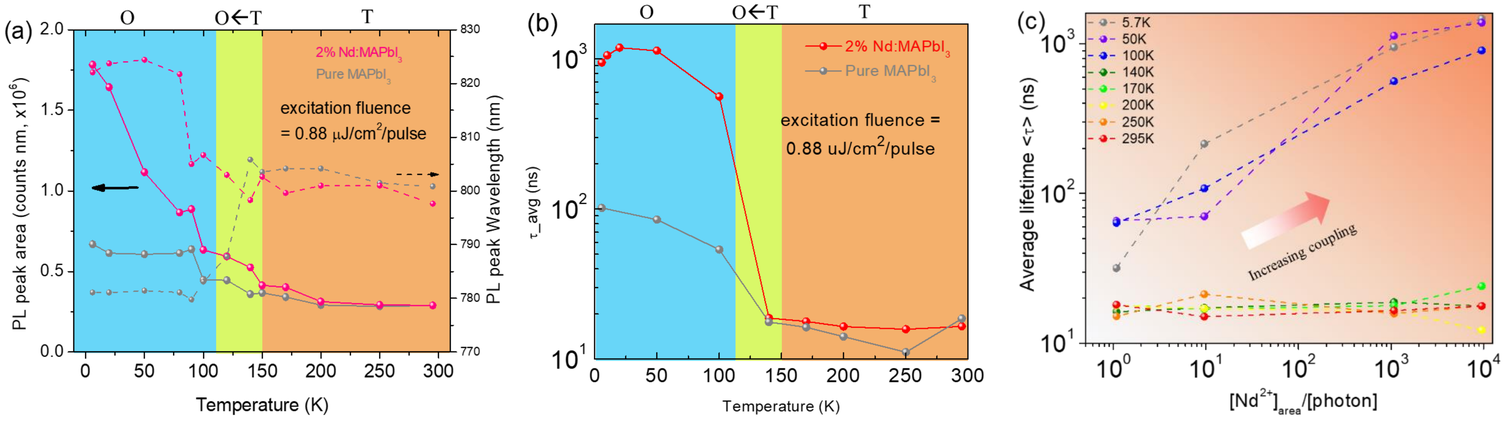

Figure 2. (a) Temperature-dependent ss-PL peak wavelength and PL intensity ratio of 2%Nd:$MAPbI_3$ to pristine $MAPbI_3$. (b) Temperature-dependent <τ> of pristine $MAPbI_3$ vs. 2%Nd:$MAPbI_3$ extracted from tr-PL decays study. (c) Summary of <τ> at different temperatures and Nd^{2+}-to-photon density ratios.

Characterization of pristine $MAPbI_3$ and 2%Nd:$MAPbI_3$

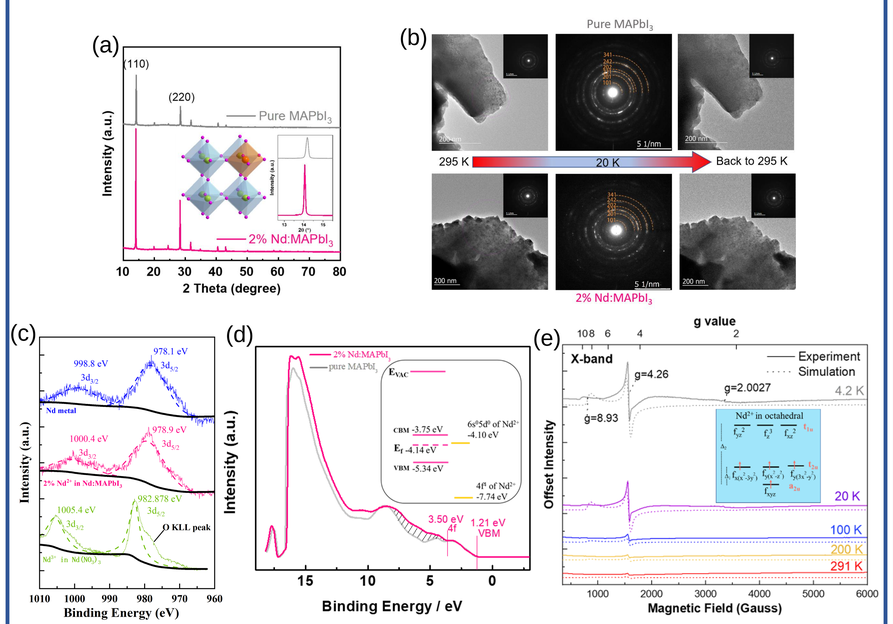

Figure 1. Characterization of pristine $MAPbI_3$ and 2%Nd:$MAPbI_3$ films. (a) XRD patterns. (b) TEM images and ED patterns at different temperatures. (c) XPS of Nd-4d for the Nd^{2+} in 2%Nd:$MAPbI_3$ vs. the Nd^{3+} in $Nd(NO_3)_3$. (d) UPS of 2%Nd:$MAPbI_3$ vs. pure $MAPbI_3$. (e) Temperature-dependent EPR spectra of grinded powder of 2%Nd:$MAPbI_3$.

PL study of pristine $MAPbI_3$ and 2%Nd:$MAPbI_3$ in magnetic field

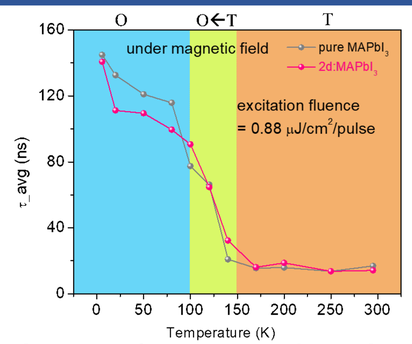

Figure 3. Temperature-dependent <τ> of pristine $MAPbI_3$ and 2%Nd:$MAPbI_3$ under magnetic field (normal to sample surface with magnetic field strength of 1500 Gauss near sample surface) extracted from tr-PL decays study.

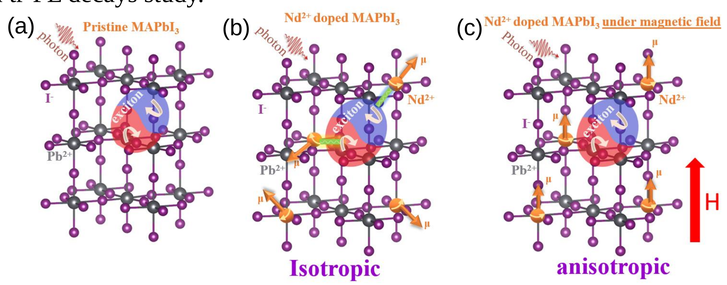

Figure 4. Schematic representation of the interplay between photoexciton and 4f impurity. (a) Recombination of photocarriers in pristine $MAPbI_3$. (b) the spin exchange interactions between the isotropic localized spins of Nd^{2+} cations with the electron and hole in the exciton. (c) In the presence of magnetic field, the localized spins on Nd^{2+} cations are anisotropically polarized, preventing the coupling between Nd^{2+} spin with either electron or hole in the exciton.

Conclusions

Divalent NdI_2 was successfully synthesized and added into pristine $MAPbI_3$ as the dopant. A markedly retarded kinetics was observed by the temperature-dependent tr-PL study of the Nd^{2+} doped hybrid perovskite.

The regulative trapping and de-trapping processes of perovskite photoelectrons have quantum-level importance, where we envision numerous frontier applications, including quantum computing, spintronics, and single-photon detection, will benefit from the meticulously engineered electronic coupling in perovskite systems as developed from this work.

References

1. A. Zhao et al., *Science* 309, 1542-1544 (2005).
2. D. Goldhaber-Gordon, et. al. Kondo effect in a single-electron transistor, *Nature*, 1998, 391, 156-159.
3. Y.-h. Zhang et al., *Nat. Commun*. 4, 2110 (2013).
4. S. M. Cronenwett, T. H. Oosterkamp, L. P. Kouwenhoven, A Tunable Kondo Effect in Quantum Dots, *Science*, 1998, 281, 540-544.
5. H. Jeong et al., *Science* 293, 2221-2223 (2001).

Acknowledgement

T.X. acknowledges the support from National Science Foundation DMR1806152 and NSF Special Creativity Award. The works performed at Argonne National Laboratory's Center for Nanoscale Materials, US DOE Office of Science User Facilities, were supported by the U.S. DOE, Office of Basic Energy Sciences, under Contract No. DE-AC02-06CH11357.

Imaging Subcellular Elemental Distribution and Morphology of Nitrogen-fixing Filamentous *Anabaena*

Bobby G. Duersch[1], Steven A. Soini[1], Yanqi Luo[2], Xiaoyang Liu[2], Si Chen[2], and Vivian M. Merk[1]

[1]Department of Chemistry and Biochemistry, Department of Ocean and Mechanical Engineering, Florida Atlantic University, Boca Raton, FL 33431
[2]X-ray Photon Sciences, Advanced Photon Source, Argonne National Laboratory, Lemont, IL 60439

Nitrogen-fixing cyanobacteria are photosynthetic microorganisms that play a critical role in the global nitrogen cycle by converting atmospheric nitrogen into organic compounds essential to many other organisms. However, there is a large fundamental knowledge gap regarding the sub-cellular distribution of trace elements across the cellular ultrastructure. This study focused on axenic cultures of *Anabaena sp.* grown in the absence of nitrogen to promote atmospheric N_2 fixation. These freshwater cyanobacteria are commonly found in subtropical climates. *Anabaena sp.* are filamentous nitrogen fixing cyanobacteria that differentiate into specialized cells: heterocysts, which fix atmospheric N_2 and transfer fixed nitrogen to adjacent cells, and vegetative, which use fixed nitrogen from heterocysts and perform oxygenic photosynthesis. Multimodal imaging techniques are essential tools for studying the structure and function of biological systems. These techniques combine different imaging modalities to provide a more comprehensive view of the system being studied. In the present study, we employed synchrotron x-ray fluorescence (XRF) under cryogenic conditions with the Bionanoprobe (Advance Photon Source, Argonne National Lab), known for its sub-100 nm spatial resolution and chemical sensitivity for a myriad of elements. By combining XRF imaging with inline optical fluorescence microscopy at the beamline, we were able to identify and localize the cyanobacteria based on chlorophyll autofluorescence. Two- and three-dimensional XRF mappings revealed distinct clusters rich in P, K, and Ca. The mappings also showed hotspots of Fe, which is a critical cofactor for the nitrogenase enzyme. Scanning Transmission Electron Microscopy (STEM) combined with EDS and XRF data were consistent with differences in trace element concentrations between cell types and the septal junction, which mediates intercellular exchange in heterocyst-forming cyanobacteria. The cell surface topology as well as the physicochemical properties of the cell surface were examined under ambient conditions using Atomic Force Microscopy (AFM). By combining these techniques, we were able to obtain high-resolution images of nitrogen-fixing *Anabaena sp*. that reflect the ultrastructure and chemical makeup.

Using Multimodal Imaging Techniques to Visualize Nitrogen-fixing Filamentous *Anabaena* sp.

Bobby G. Duersch[1], Steven A. Soini[1], Yanqi Luo[2], Xiaoyang Liu[2], Si Chen[2], Vivian M. Merk[1]

[1]Florida Atlantic University, [2]XSD, Argonne National Laboratory

PURPOSE

This study focused on axenic cultures of *Anabaena sp.* grown in the absence of nitrogen to promote atmospheric N_2 fixation. These freshwater cyanobacteria are commonly found in subtropical climates. *Anabaena* sp. are filamentous nitrogen fixing cyanobacteria that differentiate into specialized cells: heterocysts, which fix atmospheric N_2 and transfer fixed nitrogen to adjacent cells, and vegetative, which use fixed nitrogen from heterocysts and perform oxygenic photosynthesis. In the present study, we employed synchrotron X-ray fluorescence (XRF) under cryogenic conditions with the Bionanoprobe (Advance Photon Source, Argonne National Lab) combined with inline optical fluorescence microscopy at the beamline. Additionally, Scanning Transmission Electron Microscopy (STEM) combined with EDS, and Atomic Force Microscopy (AFM) was used to determine cell surface topology as well as physicochemical properties.

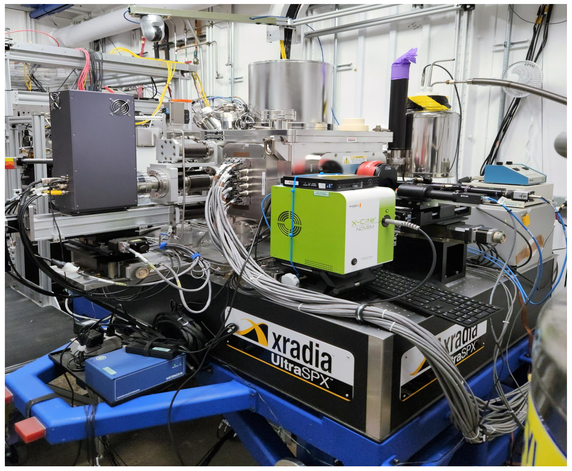

Figure 1. Bionanoprobe at the Advanced Photon Source (Argonne National Lab)

Nitrogen-fixing cyanobacteria such as *Anabaena* sp. are photosynthetic microorganisms that play a critical role in the global nitrogen cycle by converting atmospheric nitrogen into organic compounds essential to many other organisms. However, there is a large fundamental knowledge gap regarding the sub-cellular distribution of trace elements across the cellular ultrastructure.

RESULTS

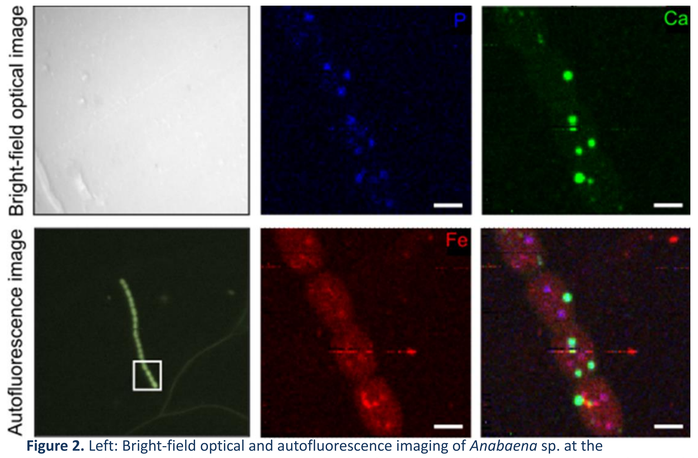

Figure 2. Left: Bright-field optical and autofluorescence imaging of *Anabaena* sp. at the Bionanoprobe, Advanced Photon Source. Right: Synchrotron X-ray Fluorescence micrographs reveal distinct hotspots of phosphorous, calcium and iron. Scale bar corresponds to 2 µm.

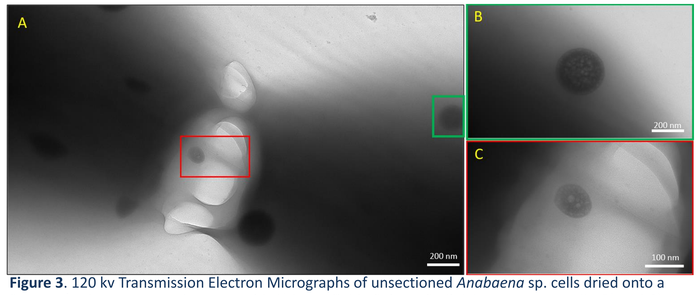

Figure 3. 120 kv Transmission Electron Micrographs of unsectioned *Anabaena* sp. cells dried onto a formvar/carbon supported copper grid. A) Large field of view of a link between two cells. B) and C) Selected areas zoomed in on lipid droplets at different locations.

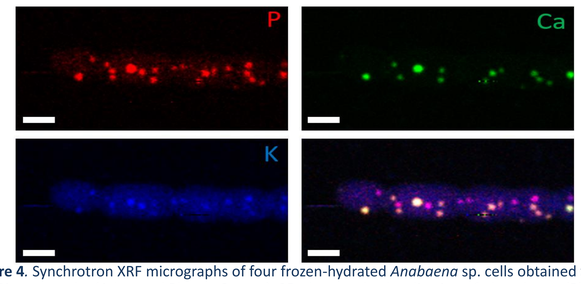

Figure 4. Synchrotron XRF micrographs of four frozen-hydrated *Anabaena* sp. cells obtained with the Bionanoprobe (Advanced Photon Source). 2D elemental colocalization of phosphorus (P), calcium (Ca), potassium (K). 100 nm step size. Scalebar corresponds to 2 µm

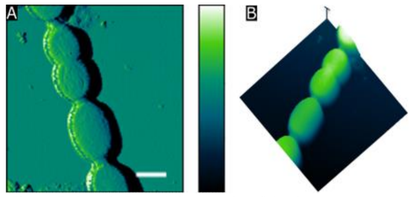

Figure 5. Atomic Force Micrographs of *Anabaena* sp. obtained in tapping mode under ambient conditions. (A) False-colored phase image. Scale bar corresponds to 2µm. (B) 3D topography image

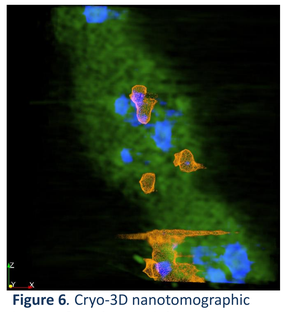

Figure 6. Cryo-3D nanotomographic image of *Anabaena*. Calcium (orange), iron (green), and potassium (blue).

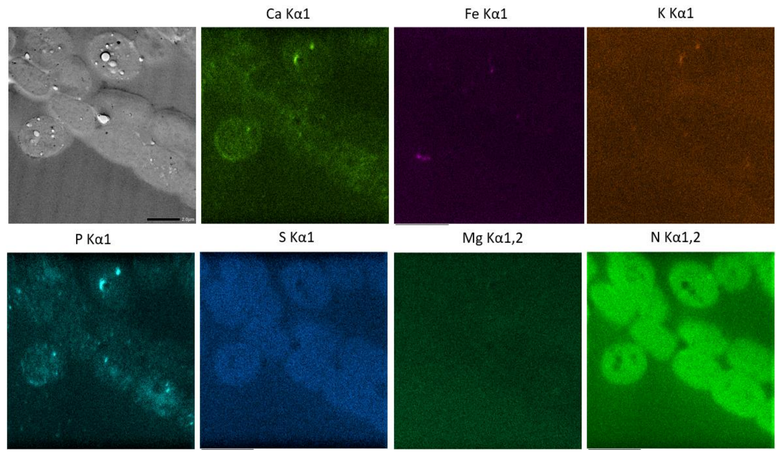

Figure 7. STEM/EDS micrographs of *Anabaena* sp. cells sectioned at 200 nm. Scale bar corresponds to 2 µm.

CONCLUSION

Multimodal imaging techniques are essential tools for studying the structure and function of biological systems. These techniques combine different imaging modalities to provide a more comprehensive view of the system being studied. We were able to identify and localize the cyanobacteria based on chlorophyll autofluorescence inline with the Bionanoprobe. Two- and three-dimensional XRF mappings revealed distinct clusters rich in P, K, and Ca. The mappings also revealed hotspots of Fe, which is a critical cofactor for the nitrogenase enzyme. STEM/EDS and XRF data were consistent with differences in trace element concentrations between cell types and the septal junction, which mediates intercellular exchange in heterocyst-forming cyanobacteria. By combining these techniques, we were able to obtain high-resolution images of nitrogen-fixing *Anabaena* sp. that reflect the ultrastructure and chemical makeup.

Acknowledgements

The authors acknowledge funding from the Walter and Lalita Janke foundation Innovations in Sustainability Science Research Grant to Dr. Merk. This research used resources of the Advanced Photon Source; a U.S. Department of Energy (DOE) Office of Science User Facility operated for the DOE Office of Science by Argonne National Laboratory under Contract No. DE-AC02-06CH11357.

Testing the Transformational Faulting Hypothesis for Deep-focus Earthquakes in the Laboratory

Jeremy Zhao[1], Timothy Officer[2], Tony Yu[2], Man Xu[2], and Yanbin Wang[2]

[1]Naperville Central High School, Naperville, IL 60540
[2]GSECARS, Advanced Photon Source, Argonne National Laboratory, Lemont, IL 60439

Until the last few decades, the mechanism by which deep-focus earthquakes (i.e., seismicity below 350 km depth) formed was still largely a mystery. Conventional brittle-fracturing no longer applies at these depths because rocks are expected to be ductile and fluid-like. One hypothesis for deep-focus earthquakes is due to phase transformation in mineral olivine, which is abundant in the upper mantle. Below ~350 km depth, olivine transforms into spinel (ringwoodite) or spineloid (wadsleyite) phases at high pressure and temperature. The high-pressure phases are fine-grained and superplastic and form shear localizations, which ultimately self-organize into large-scale fault zones. In our experiments at GSECARS, we used the deformation DIA apparatus to deform analog olivine samples Mg_2GeO_4 within the spinel stability field at high pressure and temperature. We used x-ray diffraction to determine stress and radiography to measure strain. Six acoustic emission transducers were used to detect rupture events during deformation. This poster details the process of manually picking first arrivals (the times at which the sensors detect acoustic emissions) and how it is then possible to engage in cross-correlation of the individual events' waveforms to understand how fault zones are produced during transformational faulting.

Testing the Transformational Faulting Hypothesis for Deep-focus Earthquakes in the Laboratory

Jeremy Zhao[1], Timothy Officer[2], Tony Yu[2], Man Xu[2], Yanbin Wang[2]

[1]Naperville Central High School, Naperville, IL 60540
[2]GSECARS, The University of Chicago, Argonne, IL 60439

Abstract

Until the last few decades, the mechanism by which deep-focus earthquakes (i.e., seismicity below 350 km depth) formed was still largely a mystery. Conventional brittle-fracturing cannot occur at these depths because rocks tend to become ductile and fluid-like. One hypothesis for deep-focus earthquakes is phase transformation induced embrittlement in mineral olivine, which is abundant in the upper mantle. Below ~350 km depth, olivine transforms into spinel (ringwoodite) or spineloid (wadsleyite) phases at high pressure and temperature. The high-pressure phases are fine-grained and superplastic and form shear localizations, which ultimately self-organize into large-scale fault zones. In our experiments at GSECARS (sector 13 of APS), we used the deformation DIA apparatus to deform analog olivine Mg2GeO4 within the spinel stability field at high pressure and temperature. We used x-ray diffraction to determine stress and radiography to measure strain. Six acoustic emission (AE) transducers were used to detect rupture events during deformation. This poster details the process of manually picking P-wave first arrivals (the times at which the sensors detect acoustic emissions) and how it is then possible to engage in cross-correlation of the individual events' waveforms to understand how fault zones are produced during transformational faulting.

Hypothesis

Olivine-spinel phase transformation is one of a number of proposed theories: others include dehydration embrittlement and thermal shear[1]. One argument for transformational faulting is the depth of deep-focus earthquakes correlates with the spinel stability field **(Figure 1).**

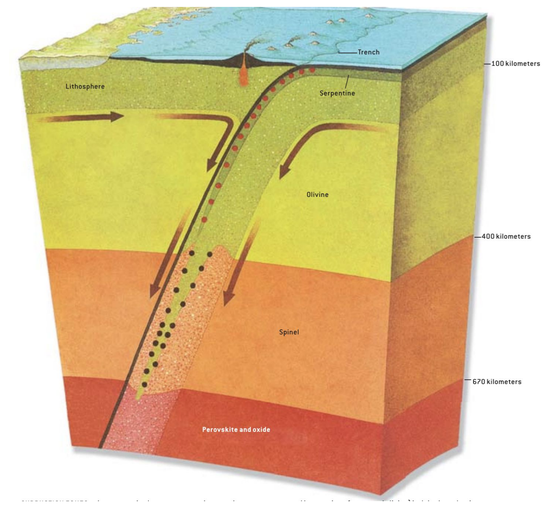

Figure 1 (Green, Scientific American, 2005)

Work Scope

To conduct laboratory simulations under controlled pressure, temperature, stress and strain rate conditions to help seismologists to understand how earthquakes nucleate. To investigate sources of errors and uncertainties in first arrival determination of the events, we conducted manual picking of ~1500 events in one experiment. The results will be further analyzed by cross-correlating waveforms to help evaluate and refine autopicking algorithms.

Methods

During experiments, six anvils, 2 polycrystalline diamond and 4 tungsten carbide (see **Figure 2)**, compress a cylindrical sample of Mg2GeO4 olivine, an analog of silicate olivine. Fastened to the rear surface of each anvil is a piezoelectric transducer capable of detecting AE events resulting from fracturing in the sample in situ.

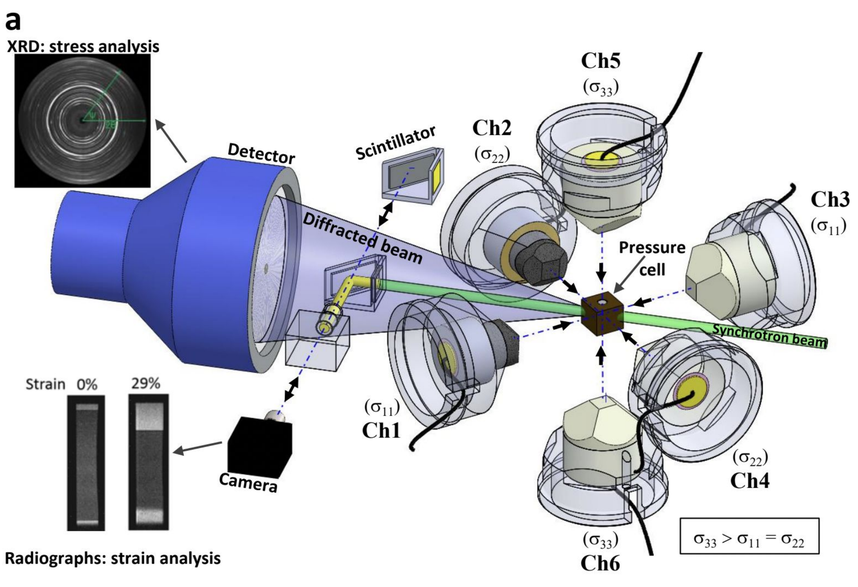

Figure 2

Data Analysis

Figure 3 displays an example of waveforms recorded by all six channels for one event. First arrivals are marked by the blue lines.

The transducers, which convert mechanical energy to electric energy, will only register the shockwave as an event when the amplitude of the waveform (volts) exceeds a pre-determined threshold. Once the software detects an event, it will include time before and after, meaning that background noise (i.e., apparatus movement, electronic noise) will show up.

After all events are manually picked, a 3D model event distribution can be created **(Figure 4)** based on the first arrival time data. Each sphere represents one event, color-coded by magnitude. This process is similar to that of detecting hypocenters of earthquakes.

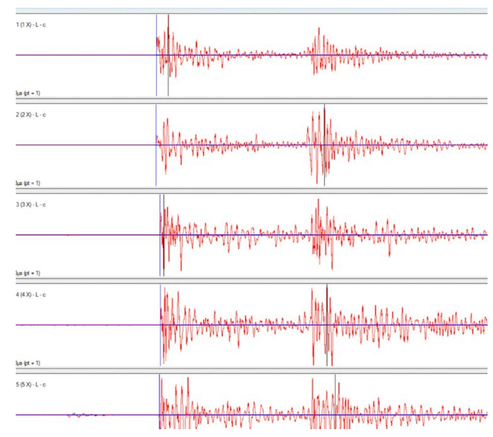

Figure 3

Accurate manual picks allow us to obtain focal mechanisms **(Figure 5)** of all events, which reveal how the fractures progressed. Each sensor can detect if the AE event is moving towards or away from it, allowing software to get a better idea of how the crack originated and developed.

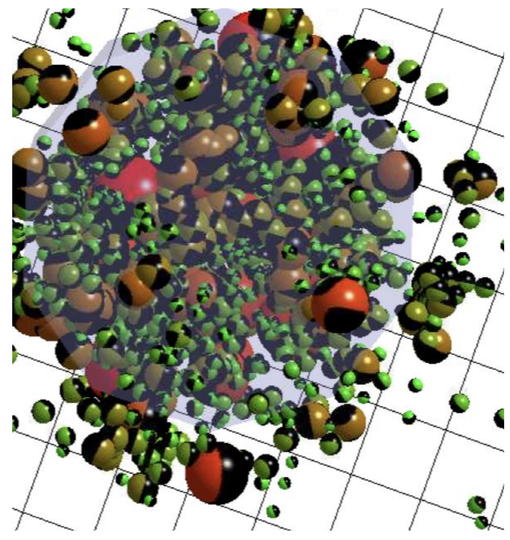

Figure 5

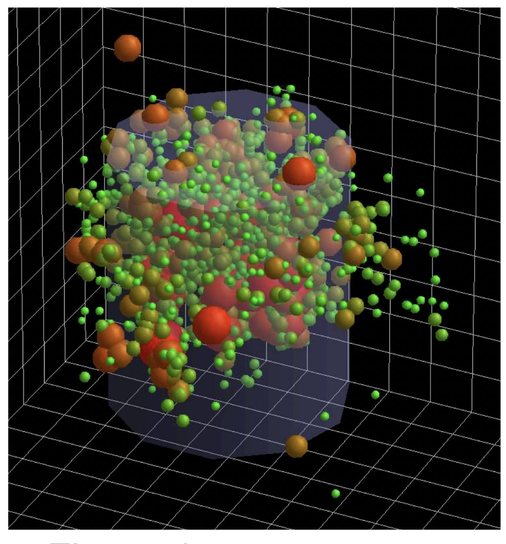

Figure 4

Conclusions

The 3D data **(Figure 4)** clearly shows several events outside the cylinder representing the sample. The scatter reflects both the noise in the system and uncertainties by manual picking of first arrivals. These data will be further analyzed using advanced seismological algorithms.

References:

[1]Li, Ziyu, 2021, A Nanoseismological Study on Acoustic Emission Events in High-Temperature and High-pressure Rock Deformation Experiments.

Interactions Between Carboxylic Acid Groups, Ions, and Water Near Interfacial Graphene Oxide

Seung Eun Lee[1], Amanda J. Carr[1], and Ahmet Uysal[1]

[1]Chemical Sciences and Engineering Division, Argonne National Laboratory, Lemont, IL 60439

Graphene oxide (GO) is a promising 2D material due to its exceptional chemical and physical properties. Therefore, there have been widely studied on rare earth separation using GO membranes. Especially, it was demonstrated that the ion separation through GO is strongly affected by the functional groups on the GO sheets. There have been countless bulk scale studies using GO in separation, but there is limited molecular scale information on ion adsorption onto the functional groups of GO.

Here, we made a very thin GO film at the air/water interface to study the effects of monovalent ions and trivalent ions on interfacial water behaviors using vibrational sum frequency generation (SFG) spectroscopy.[1] We used an arachidic acid (AA) monolayer as a benchmark to demonstrate a pure carboxylic acid surface. The SFG signals from GO peaked at the intermediate salt concentration (100 μM) with monovalent ions: LiCl, NaCl, KCl and KCl. We found that our experimental result agrees well with the modeled SFG intensities accounting for the deprotonation of the carboxylic acid groups. On the other hand, the SFG spectra from GO showed gradual decrease upon the addition of the trivalent ions.[2, 3] We also performed a $LuCl_3$ separation experiments using GO membrane in different pH.[2]. The change of the interlayer spacings of GO was characterized using x-ray diffraction data (XRD). Overall, we demonstrated that the carboxylic acid groups of GO play a major role in interfacial ion adsorption and water behaviors.

[1] Lee, S.E., et al., *Monovalent Ion - Graphene Oxide Interactions are Controlled by Carboxylic Acid Groups: Sum Frequency Generation Spectroscopy Studies*. 2023, ChemRxiv. DOI: 10.26434/chemrxiv-2023-dj4m0-v2.
[2] Carr, A.J., et al., *Effects of ion adsorption on graphene oxide films and interfacial water structure: A molecular-scale description.* Carbon, 2022. **195**: p. 131-140.
[3] Carr, A.J., et al., *Convenient Confinement: Interplay of Solution Conditions and Graphene Oxide Film Structure on Rare Earth Separations.* 2022.

Interactions between carboxylic acid groups, ions, and water near interfacial graphene oxide

Seung Eun Lee, Amanda J. Carr, Raju Kumal, Ahmet Uysal
Chemical Sciences and Engineering Division, Argonne National Laboratory, Lemont, IL 60439, United States

Scientific Objectives / Motivation

Separations with graphene oxide (GO)

[1]

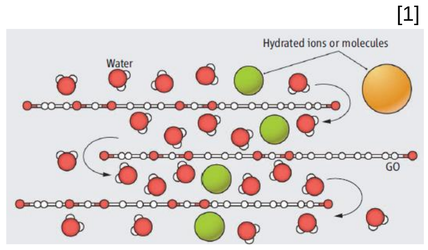

[2]

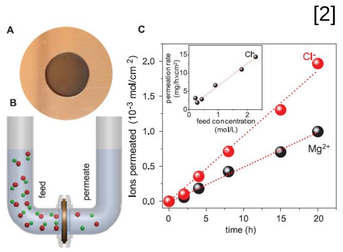

Graphene oxide (GO) is a promising separation material because of its hydrophilicity, durability, and tunable chemical properties. There have been extensive studies on ion separation, water purification, and desalination using GO membranes. Especially, it was demonstrated that the ion selectivity and permeability of GO membrane are strongly affected by the functional groups on the GO sheets.

Interfacial study is needed

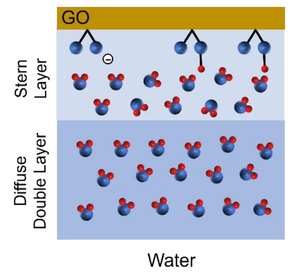

Nevertheless, most of this information is deduced from membrane scale studies. Therefore, the direct study on interfacial behaviors of the ions and water near GO functional groups is needed.

Sample Preparation

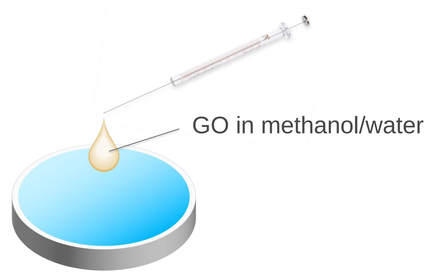

GO diluted solution (1 mg/mL with water) was diluted into methanol/water (5:1) (v/v). The resultant solution was filtered with a 1.2 μm syringe filter [3][4].
GO thin films were prepared in a polytetrafluoroethylene (PTFE) dish and the surface pressure was kept as ~20 mN/m.

Methods

Water OH Stretch band : 3000 ~ 3600 cm^{-1}

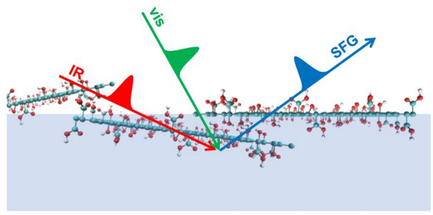

We investigated monovalent ion adsorption on GO thin films using vibrational sum frequency generation spectroscopy (SFG). SFG is a second-order nonlinear optical spectroscopy technique which probes the interfacial water organization to a few molecular layer sensitivity.

SFG Results and Discussions

SFG spectra from GO thin films with monovalent ions [5]

Water orientation increases up to 100 μM, and then disrupts gradually afterwards (100 μM ~ 1M)

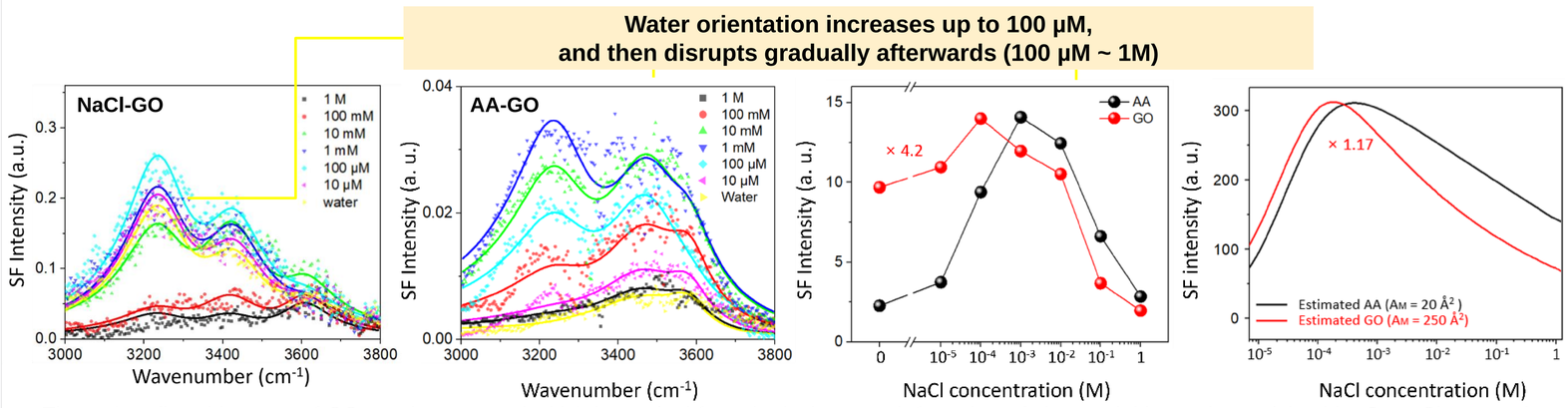

The carboxylic acid groups of GO are deprotonated which is resulted from the ionic strength from the solution, and this can be explained by Gouy-Chapman theory. SFG intensities increased from 0 M up to 100 μM of salt solutions, and started decreasing afterwards, implying that the highly ordered water orientation is formed at 100 μM of salt solution interface.

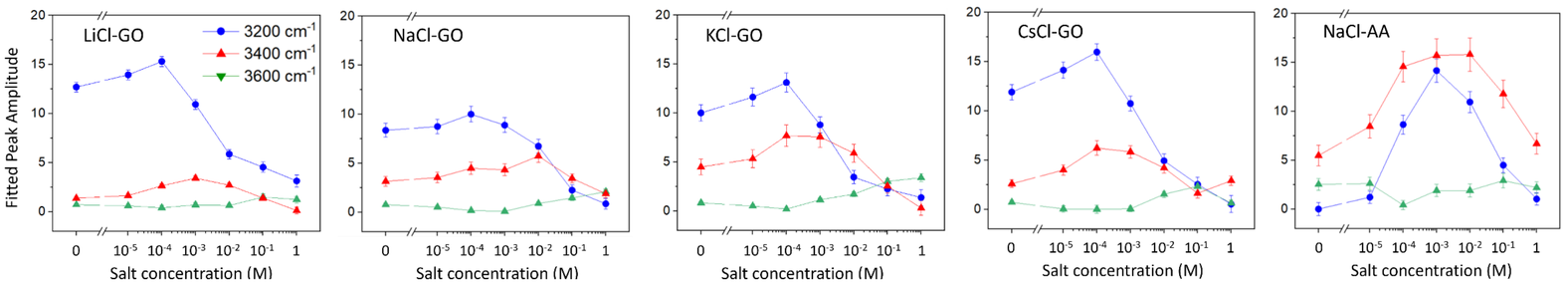

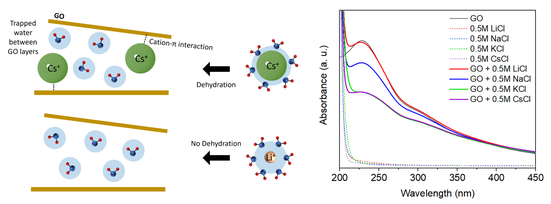

From the fitted SFG peak amplitudes for GO and AA monolayers, 3200 peak shows a similar trend to the integrated intensities while the trend for the 3400 peak are different overall. It is highly possible that the origin and distribution of these peaks are also surface dependent. We suggest that the 3400 population is very close to the surface and possibly interacting with the GO, and 3600 peak originates from the water molecules mostly trapped between the GO sheets. Interestingly, the 3600 peak is not visible from LiCl, and we posit that the Li+ retains its hydration structure and cannot intercalate between the GO layers. This hypothesis is supported by UV absorption experiments.

SFG spectra from GO thin films with trivalent ions [6]

Water signal decreases as the concentration gets higher

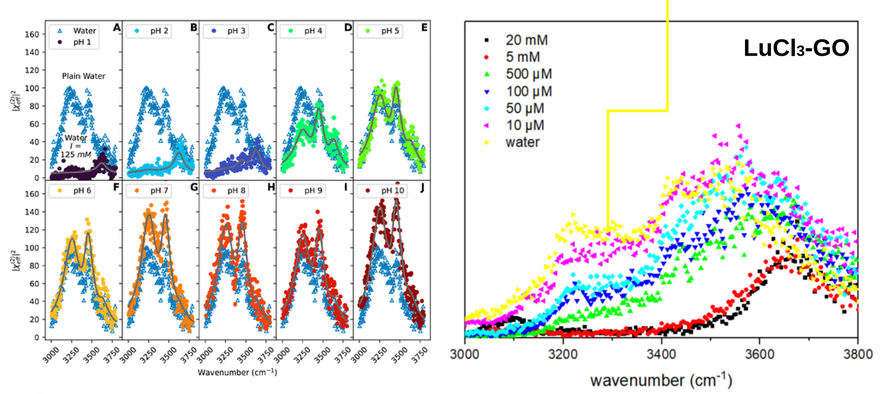

The water signals near GO films as a function of the subphase pH at fixed ionic strength was observed. The carboxylic acid groups are deprotonated as the pH gets higher. The water alignment from $LuCl_3$ solution disrupts along with the concentration gets higher, which is different from the result of monovalent ions.

Application study with GO membrane [6]

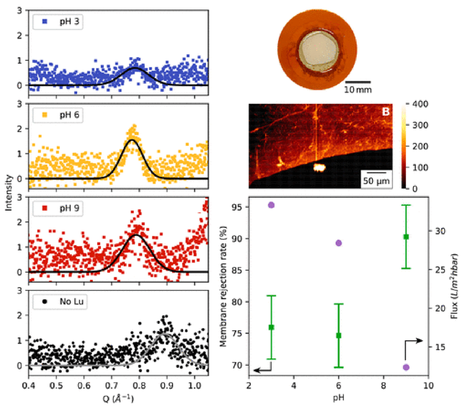

The GO membrane filtration study was performed using $LuCl_3$ at different pH. The calculated Lu3+ rejection rate was similar for feed solutions at pH 3,6 and 9 while the flux was slightly lower at pH6. XRD data on the GO membranes after filtrations show an increase in the interlayer distances compared to the plain GO membrane. Taken together, Lu3+ ions are intercalated into the GO interlayer spacings. The flux becomes the lowest at pH 9. We posit that insoluble $Lu(OH)_3$ clogs the membrane and water prevents water flow.

Conclusions

- Deprotonation of carboxylic acid groups of GO film and the consequent water orientation was confirmed by SFG measurements.
- We demonstrated the SFG shows different water orientation trend from monovalent ions and trivalent ions.
- The water orientation is affected by the amount of carboxylic acid groups and the species of functional groups.
- Ion adsorption and separation are strongly related to the water and ion behaviors at the interface, and this was demonstrated by the separation experiments using GO film.

References

[1] Baoxia Mi, Graphene Oxide Membranes For Ionic Molecular Sieving, Science, 343, 740 (2014)
[2] R. K. Joshi, P. Carbone, F. C. Wang, V. G. Kravets, Y. Su, I. V. Grigorieva, H. A. Wu, A. K. Geim , And R. R. Nair, Precise and Ultrafast Molecular Sieving Through Graphene Oxide Membranes, Science, 343, 752 (2014)
[3] Raju R. Kumal, Amanda J. Carr, Ahmet Uysal, A Simple Method for High-Quality Ultra-Thin Graphene Oxide Films Facilitates Nanoscale Investigations of Ion and Water Adsorption, preprint, ChemRxiv, 10.26434/chemrxiv-2022-1csxr (2022)
[4] Amanda J. Carr, Raju R. Kumal, Wei Bu, Ahmet Uysal, Effects of ion adsorption on graphene oxide films and interfacial water structure: A molecular-scale description, Carbon, 195, 131-140 (2022)
[5] Seung Eun Lee, Amanda J. Carr, Ahmet Uysal, Monovalent Ion - Graphene Oxide Interactions are Controlled by Carboxylic Acid Groups: Sum Frequency Generation Spectroscopy Studies, preprint, ChemRxiv, 10.26434/chemrxiv-2023-dj4m0-v2
[6] Amanda J. Carr, Seung Eun Lee, Raju R. Kumal, Wei Bu, Ahmet Uysal, Convenient Confinement: Interplay of Solution Conditions and Graphene Oxide Film Structure on Rare Earth Separations, ACS Appl, Mater. Interfaces, 14, 51, 57133-57143 (2022)

U.S. DEPARTMENT OF ENERGY
Argonne National Laboratory is a U.S. Department of Energy laboratory managed by UChicago Argonne, LLC.

Acknowledgement : This material is based upon work supported by the U.S. Department of Energy, Office of Science, Office of Basic Energy Sciences, Division of Chemical Sciences, Geosciences, and Bio-sciences, Early Career Research Program under contract DE-AC02- 06CH11357. Use of the Center for Nanoscale Materials, an Office of Science User Facility operated for the U.S. Department of Energy (DOE), Office of Science by Argonne National Laboratory, was supported by the U.S. DOE under Contract no. DE-AC02-06CH11357.

Argonne NATIONAL LABORATORY

Single-shot meV-Resolution Hard X-ray Spectrograph for CBXFEL Diagnostics

Keshab Kauchha, Peifan Liu, Paresh Pradhan, and Yuri Shvyd'ko

Advanced Photon Source, Argonne National Laboratory, Lemont, IL 60439

A cavity-based x-ray free-electron laser (CBXFEL) is a possible future direction in the development of fully coherent hard x-ray sources of high spectral brilliance, a narrow spectral bandwidth of $\sim 1 - 100$ meV, and a high repetition rate of ~ 1 MHz. A diagnostic tool is required to measure CBXFEL spectra with a meV resolution on the shot-to-shot bases. Here we present test results of a single shot hard x-ray spectrograph designed for this purpose.

A spectrograph is an optical instrument that disperses photons of different energies into distinct directions and space locations and that images photon spectra on a position-sensitive detector. Spectrographs are composed of angular dispersive and focusing optical elements.

The CBXFEL spectrograph is designed to image 9.8 keV x-rays in a ~ 200 meV spectral window and with a spectral resolution of a few meV using an LCLS XFEL source at the SLAC National Laboratory. We use Bragg reflecting Ge crystals arranged in an asymmetric scattering geometry as the dispersing elements,[1, 2] Be compound refractive lenses as focusing element,[3] and YAG-scintillator-based μm-resolution x-ray imagers.

The test experiments are performed at the Advanced Photon Source beamline 1-BM-B. The spectrograph operates close to design specification featuring a 180-meV (FWHM) spectral window of imaging and a 1.4 μm/meV linear dispersion rate. A 40-meV broad reference absorption line produced by an x-ray-transparent diamond crystal in the 440 Bragg back reflection is imaged by the spectrograph as a 45-meV broad feature, indicating a ~ 20 meV spectrograph spectral resolution.

We are grateful to Kwang-Je Kim and Lahsen Assoufid for their interest in this research work. Michael Wojcik are acknowledged for support at the Advanced Photon Source 1BM beamline. Xianrong Huang and Elina Kasman are acknowledged for manufacturing the Ge crystals for the spectrograph. Work at ANL is supported by the U.S. Department of Energy, Office of Science, Office of Basic Energy Sciences, under contract No. DE-AC02-06CH11357.

[1] Yu. Shvyd'ko. Theory of angular-dispersive, imaging hard-x-ray spectrographs. *Phys. Rev. A*, 91 (2015) 053817.
[2] A.I. Chumakov, Yu. Shvyd'ko, I. Sergueev, D. Bessas, and R Ruu¨ffer. Hard-x-ray spectroscopy with a spectrographic approach. *Phys. Rev. Lett.*, **123** (2019) 097402.
[3] B. Lengeler, C. Schroer, J. Tuu¨mmler, B. Benner, M. Richwin, A. Snigirev, I. Snigireva, and M. Drakopoulos. Imaging by parabolic refractive lenses in the hard x-ray range. *J. Synchrotron Radiation*, **6** (1999) 1153.

Single-shot meV-Resolution Hard X-ray Spectrograph for CBXFEL Diagnostics

Keshab Kauchha, Peifan Liu, Paresh Pradhan, and Yuri Shvyd'ko

Advanced Photon Source, Argonne National Laboratory, Illinois 60439, USA

Introduction

- A cavity-based x-ray free-electron laser (CBXFEL) is a possible future direction in the development of fully coherent hard x-ray sources of high spectral brilliance, a narrow spectral bandwidth of $\simeq 1-100$ meV, and a high repetition rate of $\simeq 1$ MHz. A diagnostic tool is required to measure CBXFEL spectra with a meV resolution on the shot-to-shot bases. Here we present test results of a single shot hard x-ray spectrograph designed for this purpose.
- A spectrograph is an optical instrument that disperses photons of different energies into distinct directions and space locations and that images photon spectra on a position-sensitive detector. Spectrographs are composed of angular dispersive (D) and focusing optical elements (F).
- The CBXFEL spectrograph is designed to image 9.8 keV x-rays in a $\simeq 185$ meV spectral window and with a spectral resolution of a few meV using an LCLS XFEL source at the SLAC National Laboratory. We use Bragg reflecting Ge crystals (C_1 C_2) arranged in an asymmetric scattering geometry with cumulative asymmetry parameter $b_{\cup_n} = b_1 b_2 = 1$ as the dispersing elements [1,2], Be compound refractive lenses (CRL) as focusing element [3], and YAG-scintillator-based μm-resolution x-ray imagers.

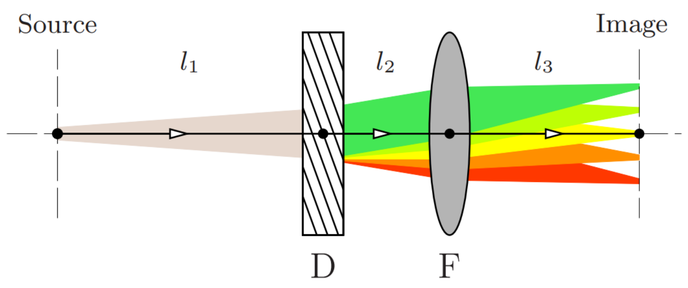

Figure 1: Principle scheme

Principle and Experimental Detail

- The spectrograph lens equation is given by: $\frac{1}{f} = \frac{1}{l_1} + \frac{1}{l_2 + l_{12} + l_3}$. Here, "$f$" is the focal length of the focusing element CRL.
- Detector Zyla camera is used for x-ray imagers and Prosilica camera is used for alignment of the CRL.

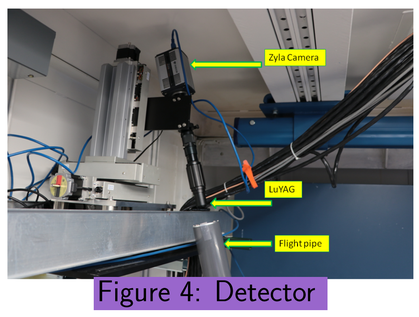

Figure 4: Detector

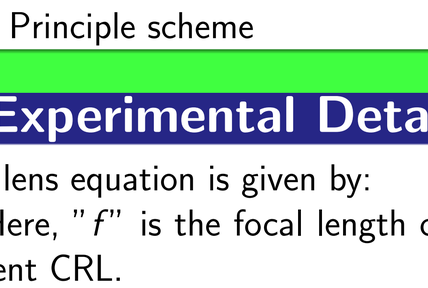

Figure 3: Experimental set-up

Figure 2: Schematic diagram

Measurements

- The measurements are done for test experiments performed at the Advanced Photon Source beamline 1BM-B. The linear dispersion rate, spectral resolution, and spectral window of imaging of the spectrograph are measured.

Linear Dispersion Rate:

- The figure below present beam images with absorption feature of diamond at various angular motion positioner.

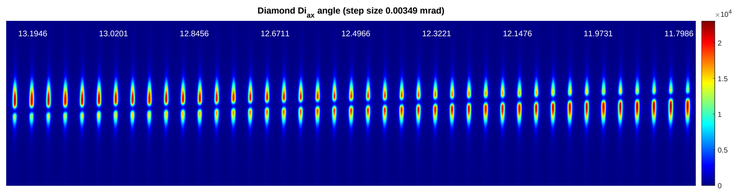

Figure 5: Beam images with absorption feature

- $(E - E_c)$ and $(\Theta - \Theta_c)$ are related by: $(E - E_c) \approx E_0\Theta_c(\Theta - \Theta_c)$. Here, $E_0\Theta_c$ is the Dumond-tangent.
- The linear dispersion rate is given by: $G_{\cup_n} = a/(E_0.\Theta_c)$. Here, "a" is the slope of the graph.

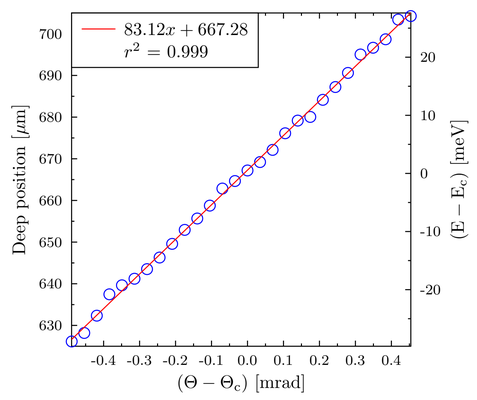

Figure 6: Deep position vs angular deviation from EBB (Exact Bragg Backscattering)

- Linear dispersion rate: $1.37\,\mu$m/meV ($E_0\Theta_c = 60.82$ meV/mrad).

Spectral Resolution:

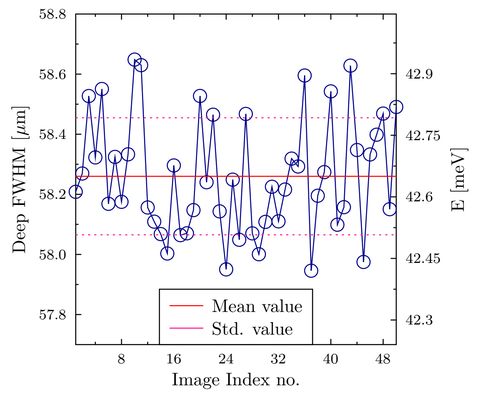

Figure 7: Deep FWHM of Image index

- Spectral broadening is: $\sqrt{42.23^2 - 40^2} = 14$ meV.

Spectral Window of Imaging:

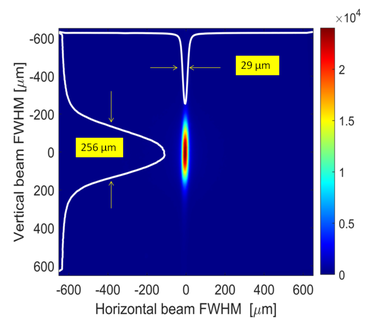

Figure 8: Horizontal and vertical beam profile

- Spectral window of imaging is: $256\,\mu$m/$1.37\,\mu$m/meV ≈ 188 meV .

Ultimate Expected Spectral Resolution :

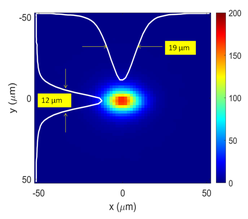

Figure 9: Horizontal and vertical beam profile

- The ultimate spectral resolution from the measurements of the source image without spectrograph is: $12\,\mu$m/$1.37\,\mu$m/meV ≈ 9 meV.

Result

- The experimentally evaluated linear dispersion rate ($1.37\,\mu$m/meV) is close to expected theoretical linear dispersion rate given by: $\frac{\delta x'}{\delta E} = l_3 \mathscr{D}_{\cup_n} \approx 1.389 \approx 1.39\,\mu$m/meV. Given, $l_3 = 1.389$ m ; $\mathscr{D}_{\cup_n} = 1\,\mu$rad/meV.
- The error bar in the measurement of linear dispersion rate is: $\pm 0.06\,\mu$m/meV.
- The evaluated value of spectral window of imaging 188 meV which is close to the theoretically expected value of 185 meV.
- The spectral resolution of our spectrograph is off by ≈ 5 meV to ultimate expected resolution.

Remarks

- We confirmed that the primary source of error responsible for degrading our spectral resolution was coming from instability of optical table.
- The sources of vibration can be minimized, and this minimization of vibration results in improved spectral resolution of the spectrograph.

Conclusion

- The spectrograph experiment performed at the Advanced Photon Source beamline 1BM-B, operates close to design specification featuring a 185-meV (FWHM) spectral window of imaging and a 1.4 μm/meV linear dispersion rate. A 40-meV broad reference absorption line produced by an x-ray-transparent diamond crystal in the 440 Bragg backreflection is imaged by the spectrograph as a 42-meV broad feature, indicating a $\simeq 15$ meV spectrograph spectral resolution.

Acknowledgement

- We are grateful to Kwang-Je Kim, Lahsen Assoufid, and Clement Burns for their interest in this research work. Michael Wojcik is acknowledged for support at the Advanced Photon Source 1BM beamline. Xianrong Huang and Elina Kasman are acknowledged for manufacturing the Ge crystals for the spectrograph. Work at ANL is supported by the U.S. Department of Energy, Office of Science, Office of Basic Energy Sciences, under contract No. DE-AC02-06CH11357.

References

[1] Yu. Shvyd'ko. Theory of angular-dispersive, imaging hard-x-ray spectrographs. *Phys. Rev. A*, **91** (2015) 053817.

[2] A.I. Chumakov, Yu. Shvyd'ko, I. Sergueev, D. Bessas, and R Ruüffer. Hard-x-ray spectroscopy with a spectrographic approach. *Phys. Rev. Lett.*, **123** (2019) 097402.

[3] B. Lengeler, C. Schroer, J. Tuümmler, B. Benner, M. Richwin, A. Snigirev, I. Snigireva, and M. Drakopoulos. Imaging by parabolic refractive lenses in the hard x-ray range. *J. Synchrotron Radiation*, **6** (1999) 1153.

[4] Bertinshaw J., Mayer S., Dill F.-U., Suzuki H., Leupold O., Jafari A., ... others. Irixs spectrograph: an ultra high-resolution spectrometer for tender RIXS. *Journal of Synchrotron Radiation*, **28**(4), (2021) 1184– 1192.

For any suggestions/queries: shvydko@anl.gov and kkauchha@anl.gov

Hiking Down the Free Energy Landscape Using Programmed Solvent and Thermal Processing for Rapid Ordering of Block Copolymer Films

Kshitij Sharma[1], Sushil Satija[3], John Ankner[4], Joseph Strzalka[5], Jack F. Douglas[2], Alamgir Karim[1]*

[1]William A. Brookshire, Department of Chemical & Biomolecular Engineering, University of Houston, TX 77204
[2]Materials Science and Engineering Division, National Institute of Standards and Technology, Gaithersburg, MD 20899
[3]NIST Center for Neutron Research, National Institute of Standards and Technology, Gaithersburg, MD 20899
[4]Structure and Dynamics of Soft Matter Group, Neutron Sciences, Oak Ridge National Laboratory, Oak Ridge, TN 37830
[5]Advanced Photon Source, Argonne National Laboratory, Lemont, IL 60439

The kinetics and morphology of ordering of block copolymer (BCP) films are highly dependent on the processing pathway methodology as the enthalpic and entropic forces driving the ordering processes can be quite different depending on process history. We show that we may gain some understanding and control of this variability of BCP morphology with processing history through a consideration of the free energy landscape of the block copolymer material and a consideration of how the processing procedure moves the system through this energy landscape in a way that avoids having the system becoming trapped into well-defined metastable minima having higher free energy than the target low free energy ordered structure. It is well-known that standard thermal annealing of BCPs leads to structures corresponding to well-defined stable free energy minima; however, the BCPs must be annealed for a very long time before the target low free energy state and structure can be achieved. Herein, we show using microscopy, GISAXS, NR, and Tof_SIMS that the same target low-energy structure can be achieved relatively quickly by subjecting as-cast films to an initial direct solvent immersion annealing (DIA) procedure, followed by a short period of thermal annealing (TA). We show that this “fast-tracked” sequential annealing process relies on allowing the BCP material to avoid becoming trapped in intermediate meta-stable free energy DIA states. Careful control of the initial DIA annealing time is required for the optimal efficiency of the overall ordering process. This energy landscape approach to ordering should be applicable to the process design for the ordering of many other complex materials.

Rapidly Ordered Vertically Oriented Block Copolymer Microstructure for Ultrafiltration Membranes

Kshitij Sharma[1], Maninderjeet Singh[1], Chenhui Zhu[2], Joe Strzalka[3], and Alamgir Karim[1]

[1]William A. Brookshire Department of Chemical & Biomolecular Engineering, University of Houston, Houston TX

[3]Advanced Photon Source, Argonne National Lab, Lemont, IL

Motivation

Water Scarcity
A Lurking Pandemic

Mitigation methods:
- ❖ Efficient Water Resources
- ❖ Planning
  - Urban Scarcity
  - National Water Needs
- ❖ Social Awareness
- ❖ Identify New Water Resources
  - Reclaim Wastewater

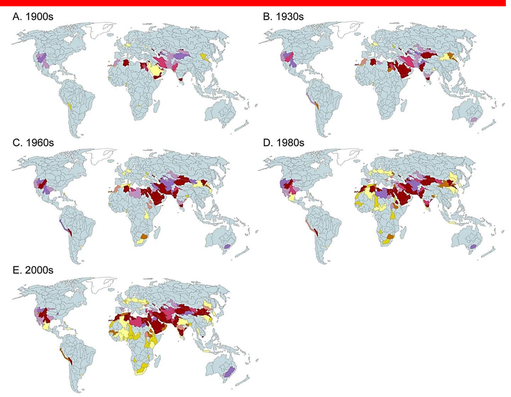

Kummu, M. et al., Sci. Rep. 6, 38495; doi: 10.1038/srep38495 (2016)

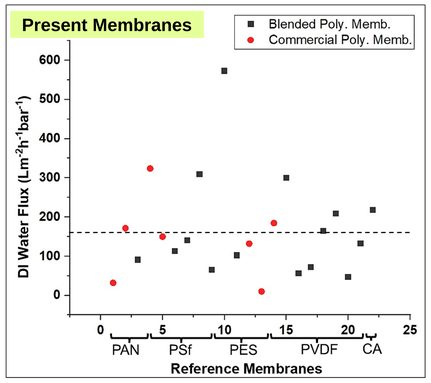

Polymer membranes
- ❖ Polymeric Membranes provide an avenue for facile energy-efficient separation processes
- ❖ Separations are not only limited to particulate matter (size-selective) but also Oil/water (wettability-selective), biomolecular (shape-selective), gaseous, and ionic (solubility based).
- ❖ Most commercial membranes are non-isoporous with highly tortuous channels

T. Ahmad et al., Journal of Water Process Engineering 36 (2020) 101289

Block Copolymers Offer a Solution

Block Copolymer (BCP) Microstructures

Diblock Copolymer

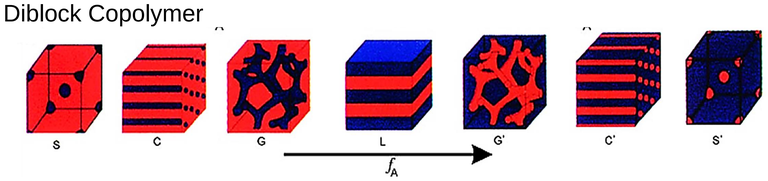

Bates et al, Phys. Today (1999), Iatrou et al., Adv. in Poly. Sci. (2005)

Membrane Potential

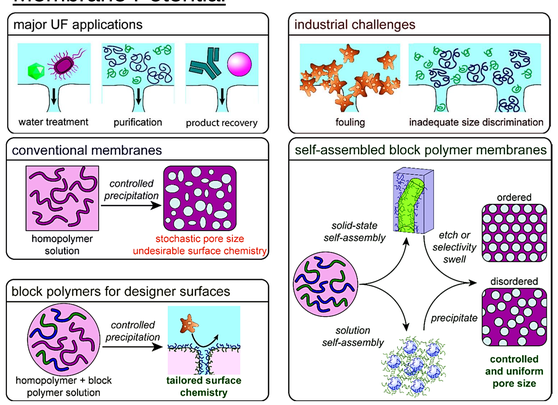

BCPs for membranes:
- ❖ Bulk membranes with non-isoporous pore surface (SNIPS)
- ❖ Bulk membranes with ordered isoporous pore surface (Substrate modification, CZA)
- ❖ Supported membranes with thin BCP active layer

Hampu et al., ACS Nano 2020, 14, 16446−16471

Morphology Development

Solvent Processing

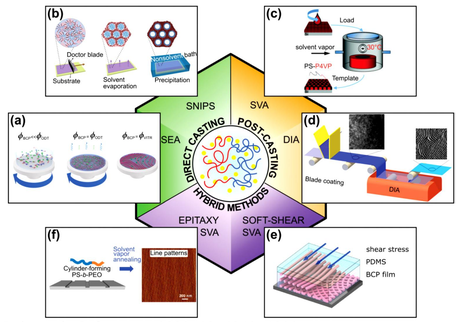

Pula et al, Soft matter, 2022, 18, 4042–4066

- ➢ Energy Efficient
- ➢ No Material loss (Capture & Recycle Solvents/Solvent Mixtures)
- ➢ Most methods still require multiple treatment steps and specific equipment, except, Solvent Evaporation Annealing (SEA)
- ➢ Materials: Polystyrene-b-Poly(methyl methacrylate) – PS-b-PMMA

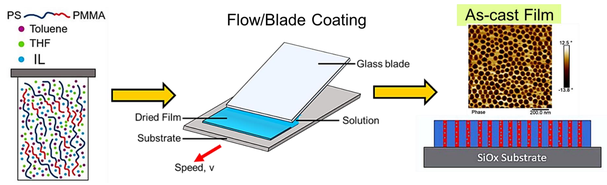

- ❖ Vertical through film channels
- ❖ Uniform domain size
- ❖ Potential for high flux

Morphology Characterization

Atomic Force Microscopy

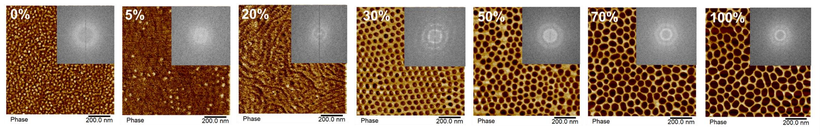

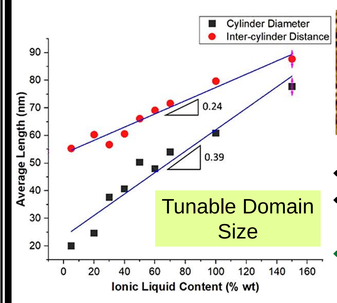

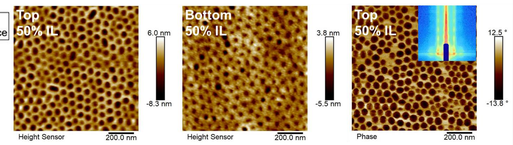

- ❖ 100 nm thick films with swollen PMMA domains
- ❖ After a critical IL content cylinders orient vertically relative to the film surface
- ❖ Both the air-polymer and substrate-polymer interfaces show vertical cylinder assembly

Grazing Incidence Small Angle X-Ray Scattering

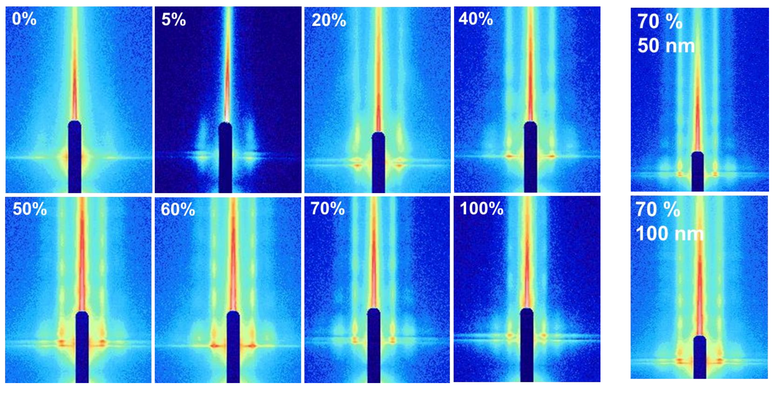

- ❖ Film thickness is 50 nm
- ❖ Increase in film thickness to 100 nm produces mixed parallel and vertical cylinders as seen from the appearance of the isotropic ring
- ❖ IL neutralizes interfacial interactions and to a higher extent in thinner films

Membrane Fabrication

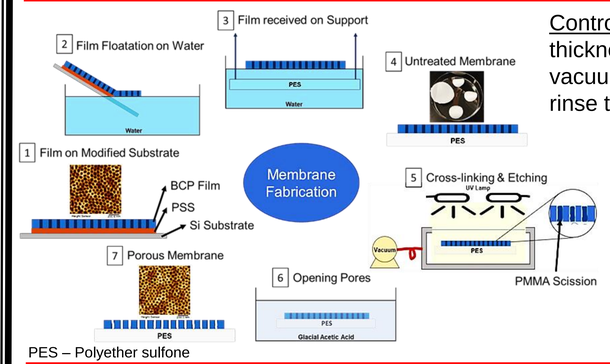

PES – Polyether sulfone

Control Parameters: Film thickness, IL content, UV vacuum time, Acetic acid rinse time, support structure

Membrane Performance

Flux Measurement

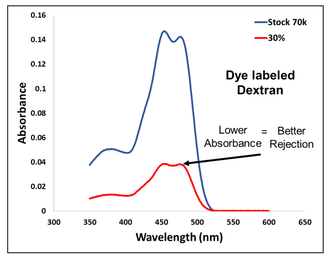

Average DI Water Flux

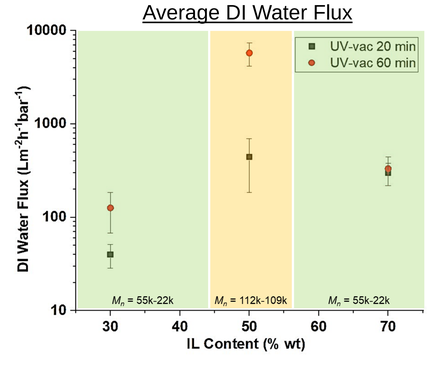

Dextran Size Cut-offs

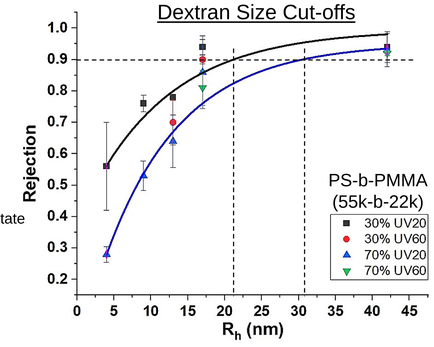

Oily Water = Water:Heptane (red dye) = 3:1

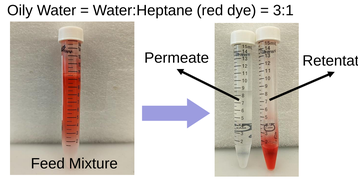

- ❖ Pore size increases with IL content and by increasing BCP M_n leading to higher fluxes and larger size cut-offs
- ❖ Extended UV-vac crosslinking improves quantity and stability of flux due to higher structural stability of the matrix PS

Conclusions

- ❖ Single-step assembly of BCP films with uniform-sized IL swollen vertical channels and facile membrane fabrication
- ❖ Tunable domain/pore sizes using variable additive content
- ❖ Higher IL contents lead to better surface neutralization for vertical order with the orientation threshold at ≈ 20 % IL content.
- ❖ Thinner films have a better vertical microstructure due to greater screening of preferential surface segregation of blocks on rapid solvent evaporation from a highly mobile film (lower T_g with IL).

Acknowledgements

The research is supported through NSF award # **1905996**. The authors would like to acknowledge the support from researchers at [2]Lawrence Berkeley and [3]Oak Ridge National Labs for GISAXS experiments and analysis.